Coverage Analysis for mmWave Networks With Reflective and Transmissive Intelligent Surfaces

Jingyuan Zhang, *Graduate Student Member, IEEE*, and Douglas M. Blough, *Senior Member, IEEE*

***Abstract*— Reconfigurable intelligent surfaces (RISs) have been proposed to enhance coverage performance in millimeter-wave bands by providing alternative links between access points and user devices in non-line-of-sight (NLOS) scenarios. However, the previously-studied reflective RISs (R-RISs) only offer 180° coverage, with most studies focusing on links with one R-RIS. Recently, transmissive-reflective RISs (T-RISs) that can provide 360° coverage have been proposed. In order to understand performance limits of both types of RISs, stochastic geometry is employed to analyze connection probability when R-RISs and T-RISs are used with single-RIS and multi-RIS links. The connection probability for single-RIS links and an upper bound on connection probability for multi-RIS links are derived with sparse obstacle distributions where independence of line-of-sight (LOS) statuses of different links can be assumed. The theoretical analysis is validated by simulations. Additionally, a comparison is provided between single-RIS and two-RIS links, as well as between R-RISs and T-RISs. Numerical evaluation using Nakagami fading propagation and a sectored antenna model shows that single-RIS links offer substantial coverage improvement for shorter-distance communications, whereas two-RIS links are more effective for longer-range communications. Moreover, numerical results demonstrate that, under the same model, T-RISs exhibit significantly improved coverage compared to R-RISs, especially with denser obstacle distribution.**

***Index Terms*— Millimeter-wave networks, transmissive intelligent surfaces, reflective intelligent surfaces, multi-RIS links, connection probability, stochastic geometry, Poisson point process.**

I. Introduction

In recent years, there has been a dramatic increase in the number of mobile devices and associated data demand, which has placed more stringent requirements on the next generation of wireless networks. Millimeter-wave (mmWave) technology, with its large bandwidth to support ultra-high network throughput, has been proposed as a critical technology to meet these requirements [1]. However, limited signal propagation distance and high penetration loss are significant challenges for mmWave communications [2], [3]. Obstacles such as furniture and even the human body can obstruct line-of-sight (LOS) paths between an access point (AP) and users, creating non-line-of-sight (NLOS) regions that reduce network coverage, particularly in moderately to highly dense obstacle environments. Recently, reconfigurable intelligent surfaces (RISs) have emerged as a novel hardware technology to provide alternative paths by redirecting signals around obstacles when no LOS path exists [4], [5].

Different types of RISs have been studied, in particular, reflective RISs (R-RISs) [6], [7], [8] and transmissive-reflective RISs (T-RISs)[1] [9], [10], [12]. R-RISs can be used to reflect signals toward any arbitrary direction, as long as the transmitter and the receiver are both on the reflective side of the RIS. T-RISs can either reflect signals or transmit signals through to the opposite side. In other words, a T-RIS can redirect incoming beams to achieve 360° signal coverage on either side of it.

Most existing work focuses on single-RIS links using R-RISs [13], [14]. Recently, a few studies have begun exploring multi-RIS links with R-RISs, with an emphasis on algorithm design for multi-RIS routing [15], [16]. However, the following questions remain unanswered.

1) Before implementing multi-RIS routing, it is essential to address whether multi-RIS links can offer more reliable connectivity. These links have the potential to enhance path diversity, allowing signals to bypass obstacles. Additionally, larger RIS array sizes can provide increased beamforming gain, compensating for signal propagation loss if an appropriate array size is selected. However, the use of multi-RIS links introduces additional overhead and delays due to the complexity of multi-RIS routing and beam alignment among multiple RISs. Therefore, it is essential to quantify the performance of multi-RIS links in order to assist cost-benefit analysis.
2) A theoretical analysis of the coverage performance of different types of RISs is essential. T-RISs offer superior signal coverage (360°) compared to R-RISs (180°), albeit with the trade-off of increased complexity for beam control. Such a theoretical analysis can provide guidance on the selection of an appropriate RIS type for a given scenario.
3) It is crucial to understand the optimal deployment of RISs for enhanced signal coverage including the number

Received 10 April 2024; revised 22 August 2024; accepted 5 October 2024. Date of publication 31 October 2024; date of current version 12 December 2024. An earlier version of this paper was presented at the 2023 IEEE LCN, Daytona Beach, FL, USA [DOI: 10.1109/LCN58197.2023.10223314]. The associate editor coordinating the review of this article and approving it for publication was Y. Liu. *(Corresponding author: Jingyuan Zhang.)*

The authors are with the School of Electrical and Computer Engineering, Georgia Institute of Technology, Atlanta, GA 30332 USA (e-mail: jingyuan@ece.gatech.edu; doug.blough@ece.gatech.edu).

Color versions of one or more figures in this article are available at https://doi.org/10.1109/TWC.2024.3486091.

Digital Object Identifier 10.1109/TWC.2024.3486091

[1] RISs that support both transmission and reflection modes are known by various names, such as simultaneous transmitting and reflecting RISs (STAR-RISs) [9], intelligent omni-surfaces [10], and transmissive-reflective RISs [11]. In this paper, we refer to these as T-RISs, indicating their ability to operate in both modes and provide 360° signal coverage.

of RISs and the appropriate array sizes, especially in terms of obstacle avoidance in mmWave networks. This requires theoretical study to uncover the relationship among coverage performance, obstacle distribution, and RIS distribution for both single-RIS and multi-RIS links.

To address the above questions, a coverage analysis framework is required to reveal the performance limits of single-RIS and multi-RIS links with different types of RISs. However, there is limited existing work on the theoretical performance analysis of RIS-assisted networks, especially in terms of obstacle avoidance and when incorporating multi-RIS links. Furthermore, there is limited theoretical work on the coverage performance of T-RISs.

In this paper, the connection probabilities of both single-RIS and multi-RIS links[2] are analyzed based on stochastic geometry, Nakagami fading, and sectored antenna models. The aim is to characterize the obstacle tolerance of RIS-assisted networks. This study on connection probability is critical as signal sensitivity to obstacles remains a primary concern for mmWave networks. We consider a scenario with a single pair of AP and user and randomly located RISs and obstacles, where obstacle density is not extremely high. The relationships among connection probability, RIS distribution, and obstacle distribution are studied to provide guidance for RIS deployment in mmWave networks. Also, comparisons are conducted to assess the relative advantages between single-RIS and multi-RIS links, as well as between R-RISs and T-RISs. The main contributions of the paper can be summarized as follows:

1) A coverage analysis framework based on stochastic geometry is provided to analyze connection probability between an AP-user pair assisted by single-RIS links and multi-RIS links using R-RISs or T-RISs, where locations of obstacles and RISs are assumed to follow spatial Poisson point processes (PPPs).
2) The connection probability between an AP-user pair assisted by single-RIS and multi-RIS links is analyzed theoretically. This analysis is conducted in scenarios with sparse obstacle distribution, where an assumption of the independence of LOS statuses on different links is valid. When this assumption holds, the exact connection probability using single-RIS links is derived and an upper bound on multi-RIS link connection probability is also proved.
3) Numerical results validate that the theoretical findings concerning the connection probability of single-RIS links closely match with simulated outcomes, especially with sparse obstacle distributions. A slight gap is observed as obstacle density rises to moderate values. The results also show that the derived upper bound is a good approximation for the two-RIS link connection probability.
4) Numerical results for single-RIS links and two-RIS links are also provided to investigate relationships among connection probability, obstacle distribution, RIS type, RIS distribution, and RIS array size. To be specific, under the assumptions of Nakagami fading and sectored antenna models:
   a) The results demonstrate that single-RIS links are efficient for improving connection probability for short-distance communication, whereas two-RIS links are more effective for longer-distance communication.
   b) Results show that, in order to reach a target connection probability between an AP-user pair, the utilization of T-RISs with 2-RIS systems[3] can reduce the size of RIS arrays, reduce RIS density, and/or increase communication distance.
   c) Results demonstrate that 1-RIS systems with T-RISs can potentially provide connection probabilities comparable to those of 2-RIS systems with R-RISs. This highlights the benefits of leveraging 1-RIS systems with T-RISs, as they effectively reduce communication overhead caused by routing and beam alignment in two-RIS links.

The paper is organized as follows. Sec. II summarizes existing research on RIS-assisted communication. Sec. III introduces preliminaries about the stochastic geometry model and received power models for RIS-assisted links, and is followed by the system model description in Sec. IV. Theoretical coverage analyses of single-RIS and multi-RIS links, respectively, are presented in Sec. V and Sec. VI. Simulation results and comparison of coverage performance of single-RIS and two-RIS links using R-RISs or T-RISs are provided in Sec. VII. Finally, Sec. VIII concludes the paper.

II. Related Work

Proposed solutions to address the mmWave band coverage issue and ensure robust connectivity include deployment of multiple APs [17], [18], relays [19], [20], [21], passive reflectors [22], [23], [24], [25] and RISs [26], [27], [28]. Multi-AP deployment reduces "NLOS regions" by placing multiple APs to provide LOS links in regions that cannot be covered by a single AP, at the expense of increased power consumption and infrastructure complexity. Multi-antenna relays, passive reflectors and RISs all try to provide indirect links by retransmitting signals from the AP to the user when there is no LOS link between them. RISs consist of an array of reflective or transmissive electromagnetic elements, e.g. metallic or dielectric particles, capable of being reconfigured to provide dynamic beam management. Therefore, RISs have the advantage of flexible beam configuration compared with passive reflectors and demonstrate benefits of low power consumption compared with multi-antenna relays [11], [29].

RISs offer a promising solution for addressing blockage issues in the mmWave band. However, it is important to have theoretical analyses of coverage performance improvement to assist network deployment. Currently, most research focuses on R-RISs, with limited studies on T-RISs. A prototype of T-RISs has been introduced in [9] with three modes: (1) full

[2] We define connection probability as the probability that a user device can be connected to an AP via either a LOS link or an RIS-assisted link with adequate received power.

[3] The M-RIS systems are defined as systems that can support LOS links and RIS links with up to M RISs.

reflection, (2) full transmission, and (3) simultaneous transmission and reflection. To explore implementation of T-RISs in communication systems, a joint optimization algorithm is proposed in [10] to optimize the beamforming scheme at the base station and the T-RIS, with the aim to maximize the sum-rate of the RIS-assisted communication system. Moreover, a comparison of sum-rate between R-RIS and T-RIS systems with single-RIS links has been demonstrated in [30]. However, current research predominantly focuses on single-RIS links assisted by T-RISs, and the coverage performance limits of T-RISs regarding obstacle avoidance in mmWave networks remain unknown.

For R-RISs, the authors in [31] theoretically analyze signal-to-noise ratio (SNR), outage probability, average bit-error rate, and ergodic capacity of multi-RIS links with the assumption of independent double generalized Gamma fading channels, which does not explicitly model obstacles in the environment. Several papers employ stochastic geometry to explicitly model obstacle distribution in RIS-assisted networks (as we do herein as well). The authors in [32] analytically derive the probability that a single R-RIS can reflect the signal between a transmitter and receiver pair with the assumption that random obstacles are coated with R-RISs which act as reflectors. However, important factors, including path loss model and received power to ensure communication quality, are not considered. In [33], the authors derive coverage probability for single-RIS links with a Boolean line model for obstacles and assuming some obstacles are coated with R-RISs. In their paper, the path loss is assumed to be proportional to $(r_1+r_2)^\alpha$, where α is the path-loss exponent, r_1 is the distance from transmitter to R-RIS, and r_2 is the distance from R-RIS to receiver. However, the model of path loss proportional to $(r_1 r_2)^\alpha$, which comports with measurements of RIS path loss from the literature [34], has been more widely used.

In this paper, the far-field path loss model is adopted for RIS links [30], [34], where the path loss is proportional to $(r_1 r_2)^\alpha$ and the far-field region is dependent on the RIS array size. Several recent papers show that there is only a small decrease in beamforming performance if a device is located in the Fresnel near-field region of an RIS compared with the case where the device is in the traditionally defined far-field region [35], [36]. According to [35] and [36], the Fresnel near-field region is the area only a few meters away from the RIS array with 128×128 elements at mmWave frequencies. It indicates that the far-field path loss is a reasonable approximation to use for network analysis, especially for mmWave networks.

To the best of the authors' knowledge, apart from the conference publication that this paper extends [37], there is no prior research studying the impact of obstacle distribution on coverage performance for both single-RIS and multi-RIS links in mmWave networks with realistic consideration of path loss model and signal strength. Moreover, the analysis of connection probability with T-RISs and the comparison of the performance between R-RISs and T-RISs have not been addressed previously. Compared to our previous conference paper, this work extends the single-RIS link and multi-RIS link analyses to scenarios with T-RISs, does an explicit comparison of the performance of T-RISs and R-RISs, and includes an evaluation of the overall coverage achievable with RISs over a given region.

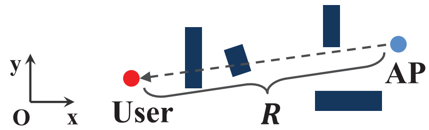

Fig. 1. Illustration of stochastic geometry model (Top view).

III. Preliminaries

Stochastic geometry is an analytical tool for evaluating network performance, where some important entities are randomly distributed in the desired region, typically according to a spatial PPP [38], [39]. Using stochastic geometry, critical network performance metrics including coverage probability and throughput can be derived via analytical expressions. This section provides background on stochastic geometry and received power model of RIS-assisted links which will be used to derive connection probability.

A. Stochastic Geometry Model

1) System Setting: Based on a widely-used system setting of stochastic geometry, a two-dimensional (2D) case is considered with one AP, one user, and randomly located obstacles as illustrated in Fig. 1. According to [38], obstacles can be modeled as random rectangles whose centers are modeled as a PPP with density μ_o on a 2D plane. Obstacle length and width are assumed to be uniform random variables with expectations $E(L)$ and $E(W)$, respectively. Moreover, the angle between the obstacle orientation and the positive direction of the x-axis is modeled as a random variable uniformly distributed between 0 and 2π.

2) LOS Probability: LOS probability, which is the probability that there exists a LOS path connecting the AP and the user, is an important metric, especially in mmWave communication where signals are extremely sensitive to blockage. When using the system setting described above, the LOS probability is [38]

$$P_l(R) = e^{-(\beta R + p)}, \tag{1}$$

where R is the horizontal distance between the AP and the user, $\beta = \frac{2\mu_o(E(L)+E(W))}{\pi}$ and $p = \mu_o E(L)E(W)$.

B. Types of RIS Studied

Two types of RISs are considered in this paper, which are described as follows:

1) R-RIS: As shown in Fig. 2(a), it features a single reflective array, allowing communication links only on one side of it.

2) T-RIS: It features a transmissive-reflective array as shown in Fig. 2(b), which can operate in transmission mode or reflection mode to redirect the beam on either side of it.

C. Received Power of RIS-Assisted Links

Considering that a user can establish a communication link to the AP if there is adequate received power, it is necessary to understand the received power model of RIS-assisted links.

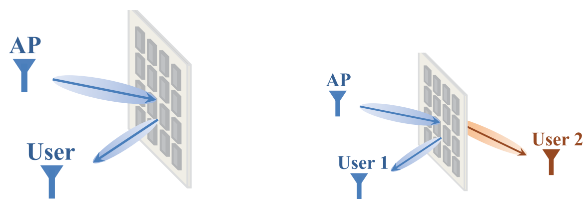

(a) R-RIS. (b) T-RIS.

Fig. 2. Illustration of R-RIS and T-RIS.

As mentioned earlier, the far-field path loss model is adopted for an RIS-aided link for coverage analysis. In what follows, let P_t denote the transmit power, λ denote the wavelength of the operational band, G_t and G_r represent the antenna gains at the AP and the user, respectively, A denote the aperture size of one RIS element, and N_k represent the number of elements on each RIS array.

Furthermore, let the Nakagami random variable h model the small-scale fading envelope on each mmWave link between two devices. From [40], the corresponding channel gain $g = h^2$ is a gamma random variable with the following probability density function:

$$f_g(x) = \frac{x^{\gamma_1 - 1} e^{-\gamma_2 x} \gamma_2^{\gamma_1}}{\Gamma(\gamma_1)}, \tag{2}$$

where γ_1 is the shape parameter, γ_2 is the inverse scale parameter in gamma distribution, and $\Gamma(\cdot)$ is the gamma function. The corresponding cumulative distribution function (CDF) is given by:

$$F_g(x) = \frac{f(\gamma_1, \gamma_2 x)}{\Gamma(\gamma_1)}, \tag{3}$$

where $f(\gamma_1, \gamma_2 x)$ is the lower incomplete gamma function. It is also assumed that the channel gains resulting from small-scale fading are independent and identically distributed (i.i.d.) across different links. For the purpose of deriving small-scale channel gain for multi-hop links, the CDF of the product of two i.i.d. gamma random variables with shape parameter γ_1 and inverse scale parameter γ_2 was shown in [41] to be:

$$F(x) = \frac{\gamma_2^{2\gamma_1}}{\Gamma^2(\gamma_1)} x^{\gamma_1} H_{1,3}^{2,1}\left({}^{1-\gamma_1}_{0,0,-\gamma_1} \middle| \gamma_2^2 x \right), \tag{4}$$

where $H_{p,q}^{m,n}(\cdot|\cdot)$ represents the Meijer G-function [42]. From [41], when γ_1 is an integer, (4) simplifies to a more mathematically convenient form as follows:

$$F(x) = \frac{(\gamma_1 - 1)!}{\Gamma(\gamma_1)} \Big(1 - \sum_{k=0}^{\gamma_1 - 1} \frac{2\gamma_2^{k+\gamma_1}}{k! \Gamma(\gamma_1)} x^{\frac{k+\gamma_1}{2}} K_{k-\gamma_1}(2\gamma_2 \sqrt{x}) \Big), \tag{5}$$

where $K_n(\cdot)$ denotes the modified Bessel function of the second kind with order n.

1) Received Power of LOS Links: The received power at the user is $P_{r,los} = P_t G_t G_r (\frac{\lambda}{4\pi R})^2 g_{los}$, where R is the LOS link length and g_{los} is the small-scale channel gain on LOS link.

2) Received Power of M-RIS Links: An M-RIS link is defined as a communication link reflected/transmitted by M RISs between two given locations. In real-world scenarios, the received power of an RIS-assisted link depends on the directions of incoming and outgoing beams with respect to RISs due to variations in the gain of RIS elements across different angles. Let $\theta \in [-\pi, \pi]$ be the angle of beam to/from the center of the RIS. For R-RISs, the normalized power gain of an individual RIS element is given by [34]

$$G(\theta) = \begin{cases} \cos(\theta), & \text{if} \quad \theta \in [-\frac{\pi}{2}, \frac{\pi}{2}], \\ 0, & \text{if} \quad \theta \in [-\pi, -\frac{\pi}{2}) \cup (\frac{\pi}{2}, \pi]. \end{cases} \tag{6}$$

The normalized power gain for T-RISs is given by [43]

$$G(\theta) = |\cos(\theta)|, \tag{7}$$

where $\theta \in [-\pi, \pi]$.

For tractability of analysis in the following sections, a simplified sector model is used. Let $\alpha_r \in [0, \pi]$ denote the 3 dB beamwidth when the realistic power gain model is $G(\theta) = \cos(\theta)$ if $\theta \in [-\frac{\pi}{2}, \frac{\pi}{2}]$. Then the simplified power gain for R-RISs is modeled as follows

$$G_s(\theta) = \begin{cases} 1, & \text{if} \quad \theta \in [-\frac{\alpha_r}{2}, \frac{\alpha_r}{2}], \\ 0, & \text{if} \quad \theta \in [-\pi, -\frac{\alpha_r}{2}) \cup (\frac{\alpha_r}{2}, \pi], \end{cases} \tag{8}$$

The simplified power gain model for T-RISs is given by

$$G_s(\theta) = \begin{cases} 1, & \text{if} \quad \theta \in [-\frac{\alpha_r}{2}, \frac{\alpha_r}{2}] \cup [-\pi, -\pi + \frac{\alpha_r}{2}] \\ & \qquad \cup [\pi - \frac{\alpha_r}{2}, \pi], \\ 0, & \text{if} \quad \theta \in [-\pi + \frac{\alpha_r}{2}, -\frac{\alpha_r}{2}) \cup (\frac{\alpha_r}{2}, \pi - \frac{\alpha_r}{2}]. \end{cases} \tag{9}$$

Therefore, the received power of an M-RIS link, where the signal is sequentially redirected by M RISs before reaching the user as shown in Fig. 3, can be modeled based on [34] and [15], [30] as follows:

$$\begin{aligned} P_{r,M} &= (\frac{G_t P_t g_1}{4\pi d_1^2}) \\ &\quad \times (\prod_{m=2}^{M+1} \frac{N_k^2 A G g_m G_s(\theta_{m-1}^r) G_s(\theta_{m-1}^t)}{4\pi d_m^2})(\frac{G_r \lambda^2}{4\pi}) \\ &= \frac{P_t G_t G_r (N_k A)^{2M}}{16\pi^2 \lambda^{2(M-1)}} \prod_{m=1}^{M+1} \frac{g_m}{d_m^2} \prod_{m=1}^{M} G_s(\theta_m^r) G_s(\theta_m^t), \end{aligned} \tag{10}$$

where g_m is the small-scale channel gain on the mth segment in the RIS link, d_m is the length of the mth segment in the RIS link as indicated in Fig. 3, $\theta_m^r, \theta_m^t \in [-\pi, \pi]$ denote the angle of beam to/from the center of RIS m, and $G = \frac{4\pi A}{\lambda^2}$ is the scattering gain of one RIS element [34].

IV. System Model and Definitions

In this section, the system model used for coverage analysis of multi-RIS links is introduced, followed by the definitions of connection probabilities for RIS-assisted communication.

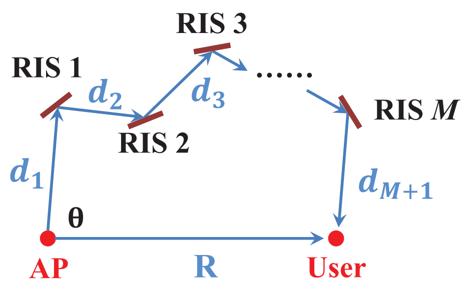

Fig. 3. Illustration of M-RIS links.

A. System Model

In this paper, we consider a 2D scenario where there is a pair of AP and user at a distance of R, and the AP, the user, centers of RISs, and obstacles are all placed in the same (X, Y) plane. Notably, the 2D model can serve as a foundational framework for exploring three-dimensional (3D) scenarios where the AP, the user, and RISs are positioned at different heights. It is assumed that each RIS array is a square array with N_k RIS elements. For each RIS element, we adopt the standard assumption that the aperture size is $A = \frac{\lambda}{2} \times \frac{\lambda}{2}$. Then, all the RISs have length $L_r = \sqrt{N_k}\frac{\lambda}{2}$ and the thickness of all the RIS arrays is denoted by W_r. Moreover, the transmit power is denoted by P_t, and the minimum received power to support a communication link is denoted by $P_{r,th}$.

As described in Sec. III-A, locations of the centers of obstacles are modeled as a homogeneous PPP with density μ_o. Herein, we add a second homogeneous PPP with density μ_r to model the locations of RIS centers. These two homogeneous PPPs are independent. The length L_o and width W_o of obstacles are uniformly distributed random variables with expectations of $E(L_o)$ and $E(W_o)$. The angle between any obstacle or RIS and the positive direction of the x-axis is modeled as a uniform random variable between 0 and 2π.

Note that this model has different PPPs for the obstacle and RIS distributions. In some prior work, e.g. [33], it is assumed that RISs are attached to obstacles and so there is one PPP, which controls the obstacle distribution. We separate these distributions for several reasons: 1) since it is not possible to attach T-RISs to obstacles without negating their transmissive capabilities, separation is necessary for T-RISs and allows us to directly compare T-RISs and R-RISs under the same conditions, and 2) separating obstacle and RIS distribution makes the model more general than the co-located scenario; in particular, with co-location, the RIS density cannot exceed the obstacle density, whereas there is no such restriction in the model considered herein. We believe R-RISs might be used even in scenarios with free-standing RISs, because they are cheaper and easier to manufacture than T-RISs.

B. Definition of Coverage Performance Metrics

In order to understand the coverage of RIS-aided systems, we analyze the connection probability, which represents the probability that the AP and the user can communicate through an unblocked link. Two different definitions of connection probability are introduced as follows:

LOS connection probability, $P_0(R)$: the probability that there exists a LOS link between an AP and a user at distance R with adequate received power at the user.

M-RIS connection probability, $P_M(D_M|R)$: the probability that there exists at least one M-RIS link to provide adequate received power at the user, given an AP and user pair at distance R, where D_M is a quantity that ensures the minimum received power to support the communication link is achieved and will be introduced later.

We further define the overall connection probability as: *Overall connection probability, $\mathcal{P}_M(R)$:* the probability that there exists a LOS link or a multi-RIS link with at most M RISs that provides adequate received power at the user, given an AP and user pair at distance R.

To quantify coverage performance in a given region, we define the coverage ratio S_M as the ratio of the area where users can communicate with the AP via either LOS links or RIS-assisted links with at most M RISs to the total area within the region.

1) LOS Connection Probability, $P_0(R)$: Different from the stochastic model introduced in Sec. III where only obstacles have impact on the LOS probability, RISs that are not selected to support RIS-assisted communication links can also interfere with the LOS path. Considering that spatial distribution of obstacles and RISs are two independent PPPs, the event that the LOS path between a pair of AP and user is blocked by obstacles and the event that the LOS path is obstructed by RISs are independent. Therefore, according to Sec. III-A.2, the LOS probability between a pair of AP and user at distance R is

$$P_{los}(R) = e^{-(\beta_o+\beta_r)R-(p_o+p_r)}, \tag{11}$$

where β_o, β_r, p_o, and p_r are given by

$$\beta_o = \frac{2\mu_o(E(L_o)+E(W_o))}{\pi}, \tag{12}$$

$$p_o = \mu_o E(L_o)E(W_o), \tag{13}$$

$$\beta_r = \frac{2\mu_r(L_r+W_r)}{\pi}, \tag{14}$$

$$p_r = \mu_r L_r W_r. \tag{15}$$

Considering the received power at the user, the connection probability of LOS links is given by

$$P_0(R) = e^{-(\beta_o+\beta_r)R-(p_o+p_r)}\left(1 - F_g\left(\frac{16\pi^2 R^2 P_{r,th}}{P_t G_t G_r \lambda^2}\right)\right), \tag{16}$$

where $F_g(\cdot)$ is defined in (3).

2) M-RIS Connection Probability, $P_M(D_M|R)$: To guarantee communication quality, the received power through an M-RIS link should be larger than the predefined threshold $P_{r,th}$. Based on the received power model introduced in Sec. III-C.2, the following condition should be met to ensure adequate received power at the user through an M-RIS link

$$\frac{\prod_{m=1}^{M+1} g_m \prod_{m=1}^{M} G_s(\theta_m^r)G_s(\theta_m^t)}{\prod_{m=1}^{M+1} d_m^2} \geq \frac{16\pi^2\lambda^{2(M-1)}P_{r,th}}{P_t G_t G_r (N_k A)^{2M}}. \tag{17}$$

For the ease of notation, the right side of (17) is denoted by D_M. Then $P_M(D_M|R)$ can be interpreted as the probability that there exists an unblocked M-RIS link which satisfies $\prod_{m=1}^{M+1} g_m \prod_{m=1}^{M} G_s(\theta_m^r) G_s(\theta_m^t) / \prod_{m=1}^{M+1} d_m^2 \geq D_M$.

3) Approximated Overall Connection Probability $\widehat{P}_M(R)$: An approximation of overall connection probability $P_M(R)$ is

$$\widehat{P}_M(R) = 1 - (1 - P_0(R)) \prod_{m=1}^{M} (1 - P_m(D_m|R)), \quad (18)$$

where dependencies between links with different numbers of RISs are ignored.

4) Coverage Ratio S_M: Considering the maximum distance R_{max} between the AP and the user, coverage ratio S_M is approximated as

$$\begin{aligned} S_M &= \frac{1}{\pi R_{max}^2} \int_0^{2\pi} \int_0^{R_{max}} \widehat{P}_M(r)\ r\,\mathrm{d}r\,\mathrm{d}\theta \\ &= \frac{2}{R_{max}^2} \int_0^{R_{max}} \widehat{P}_M(r)\ r\,\mathrm{d}r. \end{aligned} \quad (19)$$

For computational efficiency, an approximation of the coverage ratio based on Simpson's rules for integral approximation is defined as follows [44]

$$\begin{aligned} &\widehat{S}_M \\ &= \frac{2}{R_{max}^2} \frac{\Delta R}{3} \Big(\widehat{P}_M(R_1) R_1 + 4\widehat{P}_M(R_2) R_2 + 2\widehat{P}_M(R_3) R_3 \\ &\quad + 4\widehat{P}_M(R_4) R_4 + \cdots + 2\widehat{P}_M(R_{K-2}) R_{K-2} \\ &\quad + 4\widehat{P}_M(R_{K-1}) R_{K-1} + \widehat{P}_M(R_K) R_K \Big), \end{aligned} \quad (20)$$

where $R_1 < R_2 < R_3 < \cdots < R_K$ are uniformly sampled distances between the AP and the user, K denotes the number of sampled distances, and $\Delta R = R_k - R_{k-1}$ is the sampling interval.

For tractability of analysis, self-interference among different links on a multi-link path with RISs is also ignored. However, we believe that self-interference in the studied setting will be minimal for several reasons: 1) RISs are primarily used when the LOS path between the user and AP is blocked and the obstacle that blocks the LOS path also serves to block self-interference along the multi-link RIS path, and 2) in the mmWave bands, RISs and the AP should have a sufficient number of RIS/antenna elements to produce narrow beams, which will further minimize interference.

C. Notation

For ease of use, the calculation of triangle side lengths and angles used in this paper is illustrated in Fig. 4 and is defined as follows

$$d(r_1, \theta, r_2) = \sqrt{r_1^2 + r_2^2 - 2r_1 r_2 \cos\theta}, \quad (21)$$

$$\alpha_s(r_1, r_2, r_3) = \arccos(\frac{r_1^2 + r_2^2 - r_3^2}{2r_1 r_2}), \quad (22)$$

$$\alpha_a(r_1, \theta, r_2) = \arccos(\frac{r_1^2 + d^2(r_1, \theta, r_2) - r_2^2}{2r_1 d(r_1, \theta, r_2)}). \quad (23)$$

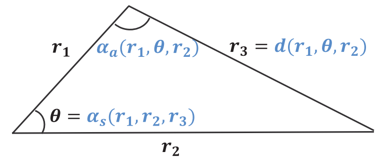

Fig. 4. Illustration of side and angle calculations in a triangle.

V. Connection Probability of Single-RIS Links

In this section, the connection probability of single-RIS links is derived analytically. For simplicity, it is assumed that the polar coordinates of the AP and the user are $(0, 0)$ and $(R, 0)$, respectively. Herein, we consider a circular region with radius L and centered at the location of AP, where only RISs and obstacles within this region are taken into account. The analysis of both single-RIS links in this section and multi-RIS links in the next section is based on an approximation that the numbers of obstacles and RISs on different links are independent, which implies that the LOS statuses of different links are independent. This is a good approximation for scenarios where RIS and obstacle distributions are not extremely dense and RISs and obstacles have relatively small sizes [33]. Note that RIS arrays can be relatively small at mmWave band, and the density of RISs will not be extremely high in practical network deployments.

Lemma 3 provides the final theoretical result on connection probability of single-RIS links. Lemma 1 and Lemma 2, stated and proved next, provide preliminary conclusions that are used in the derivation of Lemma 3.

Lemma 1 (Connection probability given RIS location): For a sparse obstacle distribution and a pair of AP and user at distance R, the probability that an RIS with polar coordinate $\boldsymbol{q} = (r, \theta)$ can provide an unblocked single-RIS link with adequate received power between the AP and the user is approximated by

$$\begin{aligned} &P_u(D_1, r, \theta | R) \\ &= H\Big(\alpha_s\big(r, d(r, \theta, R), R\big)\Big) \\ &\quad \times \Big(1 - F\big(D_1 r^2 d^2(r, \theta, R)\big)\Big) e^{-(\beta_o + \beta_r)\big(r + d(r, \theta, R)\big) - 2(p_o + p_r)}, \end{aligned} \quad (24)$$

where $F(\cdot)$ is defined in (4) or (5). Moreover, $H(\alpha)$ where $\alpha \in [0, \pi]$ for R-RISs is defined as

$$H(\alpha) = \begin{cases} \dfrac{\alpha_r - \alpha}{2\pi}, & \text{if } \alpha \leq \alpha_r, \\ 0, & \text{if } \alpha > \alpha_r, \end{cases} \quad (25)$$

and $H(\alpha)$ where $\alpha \in [0, \pi]$ for T-RISs is defined as

$$H(\alpha) = \begin{cases} \dfrac{\alpha_r - \alpha}{\pi}, & \text{if } \alpha \leq \alpha_r \text{ and } \alpha \leq \pi - \alpha_r, \\ \dfrac{\alpha_r + \alpha - \pi}{\pi}, & \text{if } \alpha > \alpha_r \text{ and } \alpha > \pi - \alpha_r, \\ \dfrac{2\alpha_r - \pi}{\pi}, & \text{if } \alpha \leq \alpha_r \text{ and } \alpha > \pi - \alpha_r, \\ 0, & \text{if } \alpha > \alpha_r \text{ and } \alpha \leq \pi - \alpha_r. \end{cases} \quad (26)$$

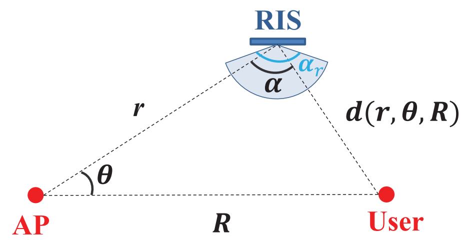

Fig. 5. Illustration of a single-RIS link.

Proof 1: For the setup illustrated in Fig. 5, the conditions that a given RIS location can provide an unblocked link with adequate received power include the occurrence of the following four events: (1) there is a LOS link between the RIS and the AP; (2) there is a LOS link between the RIS and the user; (3) the RIS has a proper orientation to redirect the beam coming from the AP to the user; (4) if the RIS has proper orientation to redirect the beam coming from the AP to the user, the received power is larger than a predetermined threshold $P_{r,th}$.

Based on (21), if the RIS is located at (r,θ), the length of RIS-AP link is given by r, and the length of RIS-user link is given by $d(r,\theta,R)$, respectively. Then the probabilities of occurrence of events (1) and (2) are given by $P_{los}(r)$ and $P_{los}(d(r,\theta,R))$, respectively, according to (11).

The probability of event (3) occurring depends on the type of RISs utilized, which is given as follows.

1) R-RIS: An R-RIS can provide a communication link when both the AP and the user are on the reflective side of it and the RIS beamwidth α_r is large enough to cover both RIS-AP link and RIS-user link. Let $\alpha \in [0,\pi]$ denote the angle between RIS-user link and RIS-AP link as illustrated in Fig. 5 and is given by

$$\alpha = \alpha_s\big(r, d(r,\theta,R), R\big). \tag{27}$$

Then the probability of event (3) occurring, denoted by $H(\alpha)$, is non-zero only when $\alpha < \alpha_r$, and is given by

$$H(\alpha) = \frac{\alpha_r - \alpha}{2\pi}. \tag{28}$$

2) T-RIS: T-RISs can support a single-RIS communication link when both the RIS-AP link and the RIS-user link fall within the sectored beam region on either side of the RIS. Similar as the derivation for R-RISs, when the angle between RIS-user link and RIS-AP link is α, the probability of event (3) occurring is given in (26).

For event (4), if the RIS is properly oriented to redirect the beam from the AP to the user, resulting in $G_s(\theta_1^r)G_s(\theta_1^t) = 1$, the condition for event (4) to occur is $g_1 g_2 \geq D_1 d_1^2 d_2^2$ according to (17). Therefore, the probability of event (4) occurring is $1 - F(D_1 d_1^2 d_2^2)$ where $F(\cdot)$ is defined in (4) or (5).

In summary, the probability of an unblocked single-RIS link with sufficient received power between the AP and the user when the RIS is located at (r,θ) is given by

$$\begin{aligned}&P_u(D_1, r, \theta|R)\\&= P_{los}(r)P_{los}(d(r,\theta,R))\\&\times H\Big(\alpha_s(r, d(r,\theta,R), R)\Big)\Big(1 - F\big(D_1 r^2 d^2(r,\theta,R)\big)\Big).\end{aligned} \tag{29}$$

Lemma 2 (Inhomogeneous PPP of effective RIS locations): For a sparse obstacle distribution, RIS locations that can provide an unblocked single-RIS link with adequate received power between a pair of AP and user at distance R are approximated by an inhomogeneous PPP denoted by $\Psi_{R,u}$ with density

$$\mu_{r,u}(D_1, r, \theta|R) = \mu_r P_u(D_1, r, \theta|R). \tag{30}$$

Proof 2: With the independence assumption of LOS statuses and small-scale channel gains on different links, the capability of different RISs to provide unblocked single-RIS links with adequate received power is independent. Therefore, those effective RIS locations form a thinned PPP[4] generated from the original PPP of RIS locations. Then the density of the thinned PPP is $\mu_r P_u(D_1, r, \theta|R)$.

Lemma 3 (Connection probability of single-RIS links): For a sparse obstacle distribution and a given pair of AP and user at distance R, connection probability of single-RIS links is approximated by

$$P_1(D_1|R) = 1 - e^{-\int_0^{2\pi}\int_0^L \mu_{r,u}(D_1,r,\theta|R) r \mathrm{d}r\, \mathrm{d}\theta}, \tag{31}$$

where D_1 is defined in Sec. IV-B.2.

Proof 3: Based on Lemma 2, which defines the distribution of effective RISs, the connection probability of single-RIS links, $P_1(D_1|R)$, can be derived by the probability that there exists at least one RIS from $\Psi_{R,u}$ defined in Lemma 2 whose location (r,θ) falls into the circular region we consider in this section.

By using the conclusion of void probability of PPP, $P_1(D_1|R)$ can be derived by the probability that all the RIS locations from $\Psi_{R,u}$ do not fall into the region defined as $\boldsymbol{S} = \{(r,\theta)|r \leq L\}$. Then the connection probability of single-RIS links is given by

$$\begin{aligned}&P_1(D_1|R)\\&= 1 - P(\mathbb{N}_{\Psi_{R,u}}(\boldsymbol{S}) = 0)\\&= 1 - \exp\left(-\int\int_{(r,\theta)\in\boldsymbol{S}} \mu_r P_u(D_1, r, \theta|R)\, r\mathrm{d}r\mathrm{d}\theta\right),\end{aligned} \tag{32}$$

where $\mathbb{N}_{\Psi_{R,u}}(\boldsymbol{S})$ denotes the number of Poisson points from $\Psi_{R,u}$ that fall into region $\boldsymbol{S}$.

VI. Connection Probability of Multi-RIS Links

In this section, the upper bound of connection probability of multi-RIS links is derived for sparse obstacle distribution. Let RIS 1 denote the RIS connected to the AP in an M-RIS link as illustrated in Fig. 3. Without loss of generality, it is assumed that the polar coordinates of the AP and the user are $(0,0)$ and $(R,0)$, respectively. A circular region with radius L is considered, with the AP at its center.

Lemma 6 provides the upper bound on connection probability of multi-RIS links with sparse obstacle distribution. Lemma 4 and Lemma 5, stated and proved next, provide preliminary conclusions used in the derivation of Lemma 6. For ease of derivation, we define two events as follows:

[4]Thinning a PPP refers to classifying each Poisson point into a number of classes based on certain stochastic rule independently [45].

Event *$A_M(D_M|R)$: there exists at least one unblocked M-RIS link that can provide adequate received power between a pair of AP and user at distance R. In other words, $P_M(D_M|R) = P(A_M(D_M|R))$ where D_M is defined in Sec. IV-B.2.*

Event *$A_M(D_M, r, \theta|R)$: there exists at least one unblocked M-RIS path that can provide adequate received power between a pair of AP and user at distance R, and RIS 1 is located at (r, θ), where D_M is defined in Sec. IV-B.2.*

Therefore, $A_M(D_M|R) = \bigcup_{\substack{r\in(0,L],\\ \theta\in[0,2\pi)}} A_M(D_M, r, \theta|R)$.

Lemma 4 (Event correlation): For sparse obstacle distribution, correlation among events $A_M(D_M, r_i, \theta_i|R)$ where $M \geq 2$ can be demonstrated by the following inequality

$$P(\bigcap_{i\in\mathbf{I}} \overline{A_M(D_M, r_i, \theta_i|R)}) > \prod_{i\in\mathbf{I}} P(\overline{A_M(D_M, r_i, \theta_i|R)}), \tag{33}$$

where $\mathbf{I}$ denotes the set of indexes of RIS 1's locations.

Proof 4: See Appendix. A.

Remark: The correlation among events $A_M(D_M, r_i, \theta_i|R)$ is intractable to be quantified, which prevents the derivation of precise connection probability for multi-RIS links. But the above inequality can be used to derive an upper bound of M-RIS link connection probability for sparse obstacle distribution. A high-level explanation of Lemma 4 is that events $\overline{A_M(D_M, r_i, \theta_i|R)}$ are positively correlated with each other. This is in line with the intuitive understanding that if there is no proper M-RIS link where RIS 1 is located at (r_i, θ_i), then the probability of there being no proper M-RIS links starting from RIS 1 near (r_i, θ_i) would increase.

Lemma 5 (Upper bound of connection probability given the first RIS location): For an AP and user pair at a distance R, if RIS 1 which is the first RIS (as shown in Fig. 3) in the M-RIS link is located at (r, θ), the upper bound of connection probability of such M-RIS links (event $A_M(D_M, r, \theta|R)$) is

$$\begin{aligned} &P\Big(A_M(D_M, r, \theta|R)\Big) \\ &< \mu_r \Delta h P_{los}(r) \\ &\times \int_0^\infty f_g(x) W_{M-1}\Big(\frac{D_M}{x} r^2, \alpha_a(r,\theta,R), d(r,\theta,R)\Big)\,\mathrm{d}x, \end{aligned} \tag{34}$$

where $\Delta h \to 0$ and $W_m(D, \alpha, R)$ is given as follows.

1) If R-RISs are used and $m \geq 2$, then

$$\begin{aligned} &W_m(D,\alpha,R) \\ &= \frac{\alpha_r}{2\pi} - \frac{\alpha_r}{2\pi}\exp\Big(\\ &\quad -\frac{\mu_r}{\alpha_r}\int_{\alpha-\alpha_r}^{\alpha}\int_0^\infty (\theta-\alpha+\alpha_r)P_{los}(r)\int_0^\infty f_g(x) \\ &\quad \times W_{m-1}\big(\frac{Dr^2}{x}, \alpha_a(r,\theta,R), d(r,\theta,R)\big) r\,\mathrm{d}x\,\mathrm{d}r\,\mathrm{d}\theta \\ &\quad -\frac{\mu_r}{\alpha_r}\int_{\alpha}^{\alpha+\alpha_r}\int_0^\infty (-\theta+\alpha+\alpha_r)P_{los}(r)\int_0^\infty f_g(x) \\ &\quad \times W_{m-1}\big(\frac{Dr^2}{x}, \alpha_a(r,\theta,R), d(r,\theta,R)\big) r\,\mathrm{d}x\,\mathrm{d}r\,\mathrm{d}\theta\Big). \end{aligned} \tag{35}$$

If R-RISs are used and $m = 1$, then

$$\begin{aligned} W_1(D,\alpha,R) = \frac{\alpha_r}{2\pi} - \frac{\alpha_r}{2\pi}\exp\Big(&\\ -\frac{\mu_r}{\alpha_r}\int_{\alpha-\alpha_r}^{\alpha}\int_0^\infty &(\theta-\alpha+\alpha_r) \\ \times P_u\big(D, r, \theta|R\big) &r\,\mathrm{d}r\,\mathrm{d}\theta \\ -\frac{\mu_r}{\alpha_r}\int_{\alpha}^{\alpha+\alpha_r}\int_0^\infty &(-\theta+\alpha+\alpha_r) \\ \times P_u\big(D, r, \theta|R\big) &r\,\mathrm{d}r\,\mathrm{d}\theta\Big). \end{aligned} \tag{36}$$

2) If T-RISs are used and $m \geq 2$, then

$$\begin{aligned} &W_m(D,\alpha,R) \\ &= \frac{\alpha_r}{\pi} - \frac{\alpha_r}{\pi}\exp\Big(\\ &-\frac{\mu_r}{\alpha_r}\int_{\alpha-\alpha_r}^{\alpha}\int_0^\infty (\theta-\alpha+\alpha_r)P_{los}(r)\int_0^\infty f_g(x) \\ &\times W_{m-1}\big(\frac{Dr^2}{x}, \alpha_a(r,\theta,R), d(r,\theta,R)\big) r\,\mathrm{d}x\,\mathrm{d}r\,\mathrm{d}\theta \\ &-\frac{\mu_r}{\alpha_r}\int_{\alpha}^{\alpha+\alpha_r}\int_0^\infty (-\theta+\alpha+\alpha_r)P_{los}(r)\int_0^\infty f_g(x) \\ &\times W_{m-1}\big(\frac{Dr^2}{x}, \alpha_a(r,\theta,R), d(r,\theta,R)\big) r\,\mathrm{d}x\,\mathrm{d}r\,\mathrm{d}\theta \\ &-\frac{\mu_r}{\alpha_r}\int_{\alpha-\alpha_r+\pi}^{\alpha+\pi}\int_0^\infty (\theta-\alpha+\alpha_r-\pi)P_{los}(r)\int_0^\infty f_g(x) \\ &\times W_{m-1}\big(\frac{Dr^2}{x}, \alpha_a(r,\theta,R), d(r,\theta,R)\big) r\,\mathrm{d}x\,\mathrm{d}r\,\mathrm{d}\theta \\ &-\frac{\mu_r}{\alpha_r}\int_{\alpha+\pi}^{\alpha+\alpha_r+\pi}\int_0^\infty (-\theta+\alpha+\alpha_r+\pi)P_{los}(r)\int_0^\infty f_g(x) \\ &\times W_{m-1}\big(\frac{Dr^2}{x}, \alpha_a(r,\theta,R), d(r,\theta,R)\big) r\,\mathrm{d}x\,\mathrm{d}r\,\mathrm{d}\theta\Big). \end{aligned} \tag{37}$$

If T-RISs are used and $m = 1$, then

$$\begin{aligned} &W_1(D,\alpha,R) \\ &= \frac{\alpha_r}{\pi} - \frac{\alpha_r}{\pi}\exp\Big(\\ &-\frac{\mu_r}{\alpha_r}\int_{\alpha-\alpha_r}^{\alpha}\int_0^\infty (\theta-\alpha+\alpha_r) \\ &\times P_u\big(D, r, \theta|R\big) r\,\mathrm{d}r\,\mathrm{d}\theta \\ &-\frac{\mu_r}{\alpha_r}\int_{\alpha}^{\alpha+\alpha_r}\int_0^\infty (-\theta+\alpha+\alpha_r) \\ &\times P_u\big(D, r, \theta|R\big) r\,\mathrm{d}r\,\mathrm{d}\theta \\ &-\frac{\mu_r}{\alpha_r}\int_{\alpha-\alpha_r+\pi}^{\alpha+\pi}\int_0^\infty (\theta-\alpha+\alpha_r-\pi) \\ &\times P_u\big(D, r, \theta|R\big) r\,\mathrm{d}r\,\mathrm{d}\theta \\ &-\frac{\mu_r}{\alpha_r}\int_{\alpha+\pi}^{\alpha+\alpha_r+\pi}\int_0^\infty (-\theta+\alpha+\alpha_r+\pi) \\ &\times P_u\big(D, r, \theta|R\big) r\,\mathrm{d}r\,\mathrm{d}\theta\Big). \end{aligned} \tag{38}$$

Proof 5: See Appendix. B.

Lemma 6 (Upper bound of connection probability of multi-RIS links): For a sparse obstacle distribution and a given pair of AP and user at distance R, the upper bound of connection probability of M-RIS links ($M \geq 2$) is given as follows

$$\begin{aligned} &P_M(D_M|R) \\ &< 1 - \exp\Big(- \mu_r \int_0^{2\pi} \int_0^L e^{-(\beta_o+\beta_r)r-(p_o+p_r)} \int_0^\infty f_g(x) \\ &\quad \times W_{M-1}\big(\frac{r^2 D_M}{x}, \alpha_a(r,\theta,R), d(r,\theta,R)\big) r \,\mathrm{d}x \,\mathrm{d}r \,\mathrm{d}\theta \Big), \end{aligned} \tag{39}$$

where $W_m(D, \alpha, R)$ is defined in Lemma 5.

Proof 6: Since $A_M(D_M|R) = \bigcup_{\substack{r\in(0,L],\\ \theta\in[0,2\pi)}} A_M(D_M, r, \theta|R)$, we have

$$\begin{aligned} P_M(D_M|R) &= 1 - P(\overline{A_M(D_M|R)}) \\ &= 1 - P(\bigcap_{\substack{r\in(0,L],\\ \theta\in[0,2\pi)}} \overline{A_M(D_M, r, \theta|R)}). \end{aligned} \tag{40}$$

Based on Lemma 4, it can be derived that the upper bound of (40) is

$$\begin{aligned} &P_M(D_M|R) \\ &< 1 - \prod_{\substack{r\in(0,L],\\ \theta\in[0,2\pi)}} P(\overline{A(D_M, r, \theta|R)}) \\ &= 1 - \prod_{\substack{r\in(0,L],\\ \theta\in[0,2\pi)}} \exp\Big(- \mu_r \Delta h P_{los}(r) \\ &\quad \times \int_0^\infty f_g(x) W_{M-1}\big(\frac{r^2 D_M}{x}, \alpha_a(r,\theta,R), d(r,\theta,R)\big) \mathrm{d}x \Big) \\ &= 1 - \exp\Big(- \mu_r \int_0^{2\pi} \int_0^L e^{-(\beta_o+\beta_r)r-(p_o+p_r)} \int_0^\infty f_g(x) \\ &\quad \times W_{M-1}\big(\frac{r^2 D_M}{x}, \alpha_a(r,\theta,R), d(r,\theta,R)\big) r \,\mathrm{d}x \,\mathrm{d}r \,\mathrm{d}\theta \Big). \end{aligned} \tag{41}$$

Before reporting numerical results on connection probability in the next section, we note that despite the above expression being valid for $M > 1$, we only report multi-RIS link results for $M = 2$. This is because of the complexity of evaluating this expression, which is a recurrence equation involving a multiple integral at each level. The number of integrals in the final expression makes the computation time extremely large to generate even a single data point for $M > 2$. However, we are still able to use the expression to evaluate, for the first time, an upper bound on connection probability for 2-RIS links.

VII. Numerical Results

In Sections VII-A and VII-B, simulation results are provided to validate: (1) the connection probability of single-RIS links presented in Lemma 3, and (2) the upper bound of connection probability of multi-RIS links from Lemma 6. Following that, in Sec. VII-C, a comparison of the coverage improvement using single-RIS links and two-RIS links is provided based on the approximated overall connection probability presented in (18). It should be noted that all results and conclusions in this section hold under the models used to derive connection probabilities in the two previous sections, namely Poisson-distributed RISs and obstacles, Nakagami fading, and the sectored antenna model.

Herein, two-RIS links are considered as a representative case for multi-RIS scenarios, since multi-RIS links with more RISs will incur a heavy overhead resulting from beam alignment and routing. For all results in this section, a mmWave network operating at 60 GHz is simulated. The equivalent isotropically radiated power (EIRP) for the AP is assumed to be 43 dBm, the received power threshold is assumed to be $P_{r,th} = -59$ dBm and the antenna gain at the user is set as 11 dB. The obstacle size is selected to model typical indoor objects, such as furniture. Therefore, the obstacle length and width are assumed to be uniform random variables with ranges [0.8 m, 1.2 m] and [0.4 m, 0.6 m], respectively. Moreover, the width and length of RISs are chosen as $W_r = 0.05$ m, and $L_r = \sqrt{N_k}\frac{\lambda}{2}$. Let R denote the distance between the AP and the user, with $R = 30$ m and $R = 150$ m chosen to represent short-distance and long-distance communication, respectively. The shape parameter γ_1 and the inverse scale parameter γ_2 in gamma distribution used to model small-scale fading are selected as $\gamma_1 = \gamma_2 = 3$.

A. Validation of Connection Probabilities of Single-RIS Links

In this subsection, the analysis of single-RIS links from Lemma 3 is compared to simulation results. We study two obstacle densities: $\mu_o = 0.05/m^2$ and $\mu_o = 0.01/m^2$, and three RIS densities: $\mu_r = 0.03/m^2$, $\mu_r = 0.005/m^2$, and $\mu_r = 0.001/m^2$. Herein, μ_r and μ_o indicate the expectation of the number of RISs and obstacles per m^2, respectively.

Fig. 6 and Fig. 7 show the relationship between RIS size and connection probability for single-RIS links for two different AP-user distances when different types of RISs are used. The very small difference in the figures between the theoretical analysis and simulation results indicates that the approximated connection probability in Lemma 3 provides a very good approximation. When comparing the connection probabilities of the two RIS types, T-RISs, with the most flexibility to support communication links, consistently demonstrate higher connection probability for single-RIS links across all selected combinations of μ_r and μ_o, as compared to R-RISs. Alternatively, one can achieve the same connection probability between T-RISs and R-RISs but with a smaller array in the T-RISs.

For RIS sizes that are practical with current technology (e.g., 32 × 32), the single-RIS link connection probability shows moderate benefits for R-RISs and quite significant benefits for T-RISs at the shorter distance, but little to no benefit for the longer distance for both types of RISs. At the shorter distance, when the obstacle density is high ($\mu_o = 0.05/m^2$), it is effective to increase RIS density to produce a good connection probability. However, increasing RIS size by itself results in a plateau of connection probability. At the longer distance, single-RIS links hardly provide any benefits with the denser obstacle distribution ($\mu_o = 0.05/m^2$) even if the RIS density increases to $\mu_r = 0.03/m^2$.

B. Validation of Connection Probabilities of Two-RIS Links

For the same two distances, Fig. 8 and Fig. 9 demonstrate the relationship between RIS size and connection probability for two-RIS links when using different types of RISs, where

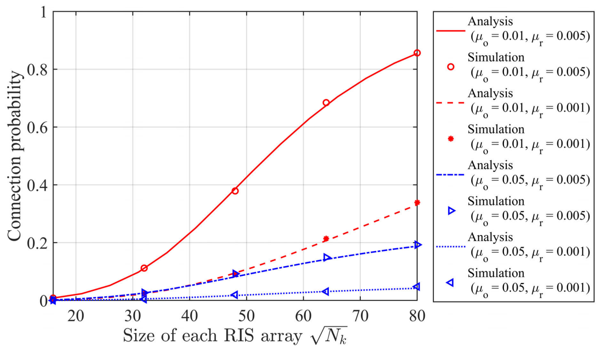

(a) $R = 30$ m.

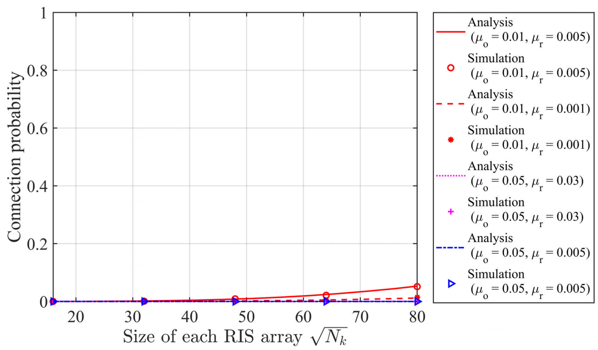

(b) $R = 150$ m.

Fig. 6. Connection probability of single-RIS links using R-RISs vs. RIS size (number of elements on each RIS array is N_k).

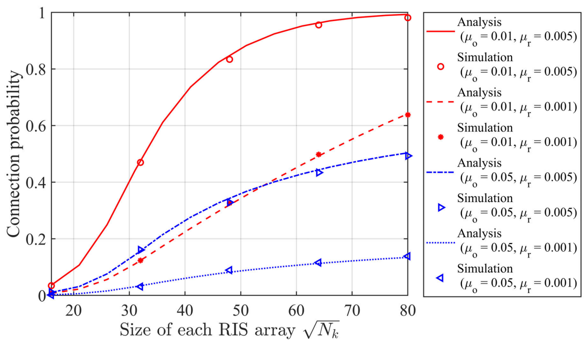

(a) $R = 30$ m.

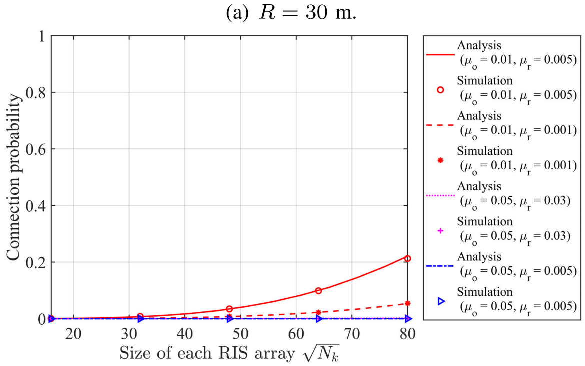

(b) $R = 150$ m.

Fig. 7. Connection probability of single-RIS links using T-RISs vs. RIS size (number of elements on each RIS array is N_k).

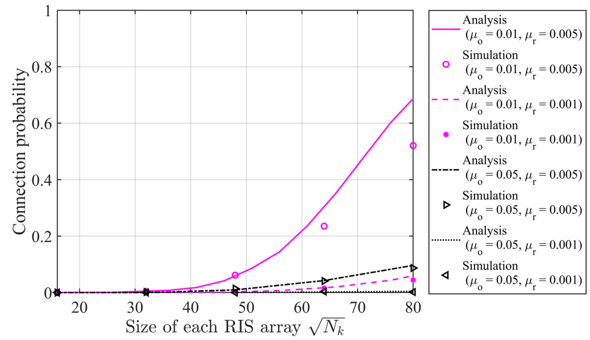

(a) $R = 30$ m.

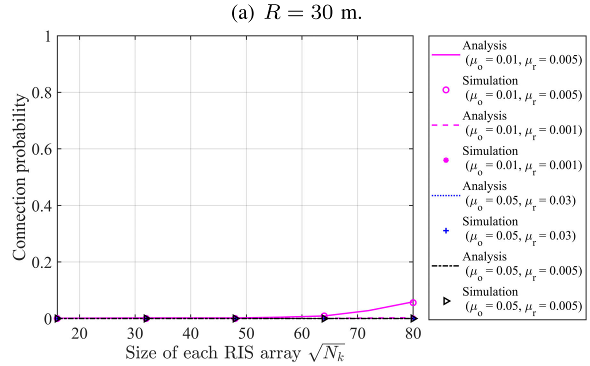

(b) $R = 150$ m.

Fig. 8. Connection probability of two-RIS links using R-RISs vs. RIS size (number of elements on each RIS array is N_k).

the theoretical curve is the approximated upper bound on connection probability derived in Lemma 6. As compared to Fig. 6 and Fig. 7, the gap between theoretical analysis and simulation is larger here. Nevertheless, the approximated upper bound and the simulation results still match fairly well in all cases for the obstacle densities studied. At the longer distance, two-RIS links provide significant connection probability improvement with a sparse obstacle distribution ($\mu_o = 0.01/m^2$) when there is adequate RIS density ($\mu_r = 0.005/m^2$) and T-RISs are utilized. This highlights the advantages of two-RIS links over single-RIS links and T-RISs over R-RISs. When obstacle distribution is denser ($\mu_o = 0.05/m^2$), two-RIS links still provide better connection probability for longer-distance communication compared to single-RIS links when RIS density is $\mu_r = 0.03/m^2$, although the connection probability remains low. However, the RIS benefit is achieved with large RIS arrays (e.g., 80×80). As with single-RIS links, T-RISs demonstrate higher connection probability as compared to R-RISs of the same size or, alternatively, the same connection probability with smaller array size. Notably, T-RISs with large array size show some benefit even for the highest obstacle density, whereas R-RISs show no benefit in that scenario.

Based on Fig. 6–Fig. 9, both single-RIS and two-RIS links can provide significant connection probability with sparse obstacle distribution if RIS sizes and densities are appropriately chosen. Moreover, from Fig. 6(a), Fig. 7(a), Fig. 8(a) and Fig. 9(a), no significant improvements of two-RIS links are observed compared with single-RIS links for short-distance transmissions. However, when comparing Fig. 6(b), Fig. 7(b), Fig. 8(b) and Fig. 9(b), note that two-RIS links gradually outperform single-RIS links for longer-distance transmissions as RIS size increases. As RIS size increases, the larger beamforming gain allows the two-RIS links to meet the required received power threshold and since two-RIS links provide

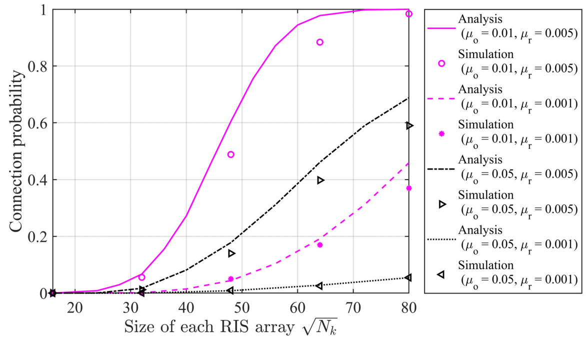

(a) $R = 30$ m.

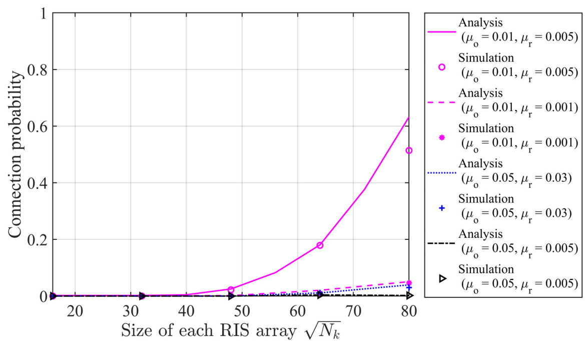

(b) $R = 150$ m.

Fig. 9. Connection probability of two-RIS links using T-RISs vs. RIS size (number of elements on each RIS array is N_k).

more opportunity for blockage avoidance, they outperform single-RIS links in that situation.

C. Overall Connection Probability Improvement

In this section, the approximated overall connection probability in (18) is investigated for a more comprehensive analysis of coverage improvement with RIS links. Note that connection probability of single-RIS links in Lemma 3 and upper bound for two-RIS links according to Lemma 6 are used to approximate the overall connection probability. Herein, 1-RIS systems are defined as systems that can support the LOS link and single-RIS links, while 2-RIS systems can support the LOS link, single-RIS links, and two-RIS links. Simulation results and theoretical analyses are shown in Fig. 10. In this section, we focus on the case where $\mu_o = 0.01/m^2$ and $\mu_r = 0.005/m^2$, so the sparse obstacle assumption holds.

Based on Fig. 10, despite the gap between theoretical analysis and simulation results, the theoretical connection probability still provides the following beneficial insights into comparison between 1-RIS and 2-RIS systems when different types of RISs are used.

(1) Effectiveness of 1-RIS systems for short-distance communication: For shorter transmission distances (Fig. 10(a) and Fig. 10(c)), 1-RIS systems can achieve perfect connection probability with sufficiently large RIS sizes. To reach overall connection probability around 0.9, the RIS array size should be approximately 64×64 for R-RISs and 36×36 for T-RISs, which demonstrates the efficiency and practicality of using T-RISs. Meanwhile, 2-RIS systems hardly produce any improvement compared with 1-RIS systems in this case for both types of RISs, indicating the effectiveness and efficiency of single-RIS systems for short-range communication.

(2) Effectiveness of 2-RIS systems for longer-distance communication: For longer-distance communication (Fig. 10(b) and Fig. 10(d)), 2-RIS systems have a significant advantage compared to 1-RIS systems and LOS communication with T-RISs, while R-RISs only show limited improvement. When RIS array size is larger than 48×48, two-RIS systems with T-RISs show nearly twice the improvement with respect to systems without RISs in overall connection probability compared to 1-RIS systems with T-RISs.

(3) Reduced RIS array size when T-RISs are used: T-RISs show better connection probability in both short and long-distance communications and their advantage becomes particularly pronounced in longer-distance scenarios where LOS connection probability is quite low. Therefore, T-RISs offer the potential to reduce the size of RIS arrays compared to R-RISs, when aiming for a desired connection probability. This can potentially reduce hardware complexity or cost to deploy RIS systems if T-RISs are used. For example, to achieve a connection probability of 0.9 over a 30 m distance between the AP and the user as shown in Fig. 10(a) and Fig. 10(c), an R-RIS array needs to be nearly 64×64, whereas employing T-RISs could reduce this size to around 36×36. In cases where the AP-user distance increases to 150 m as illustrated in Fig. 10(b) and Fig. 10(d), the array size for T-RISs can be kept within 80×80 to achieve a connection probability of 0.6, while R-RISs would require significantly larger arrays, given that R-RISs with array size 80×80 only yield approximately 0.23 connection probability.

According to Fig. 10, significant overall coverage improvement is observed with large-sized RISs, while there is hardly any improvement observed with small-sized RISs at the selected RIS density. To investigate the coverage improvement offered by RISs of more practical sizes, the approximated overall connection probability is investigated using medium-sized RISs with 64×64 array sizes at an RIS density of $\mu_r = 0.005/m^2$.

In Fig. 11, the relationship between overall connection probability and the AP-user distance is demonstrated, considering obstacle densities (μ_o) of $0.05/m^2$ and $0.01/m^2$. The following observations can be made based on Fig. 11:

(1) 1-RIS system with T-RISs vs. 2-RIS system with R-RISs: In both scenarios with sparse and dense obstacle distributions, T-RISs consistently demonstrate better connection probabilities compared to R-RISs. Furthermore, given the parameters selected for Fig. 11, the connection probability of 1-RIS systems with T-RISs always outperforms that of 2-RIS systems with R-RISs. This advantage stems from the ability of T-RISs to support communication links on both sides, thus providing increased flexibility in path selection. ***This finding highlights that, in practical systems where the overhead of routing and beam alignment in multi-RIS links is a critical consideration, use of 1-RIS links with T-RISs may be advantageous.***

(2) Enhancement in communication distance using T-RISs: The connection probability has a significant decrease with distance, especially under higher obstacle densities. We define a cut-off distance, beyond which the overall connection

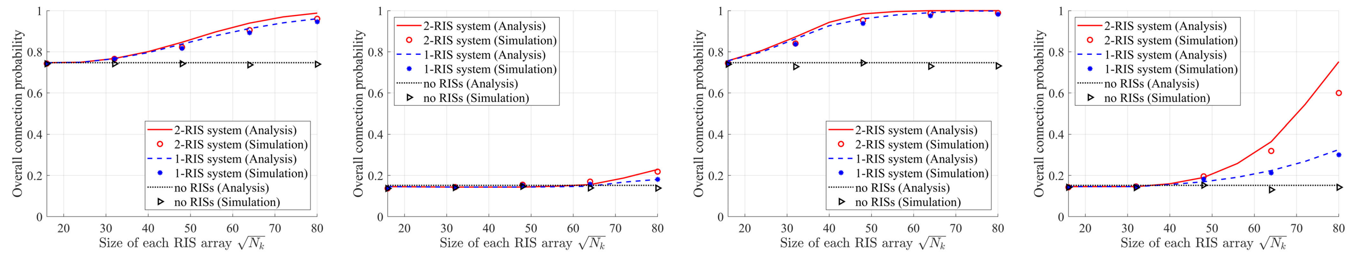

(a) R-RISs, $R = 30$ m. (b) R-RISs, $R = 150$ m. (c) T-RISs, $R = 30$ m. (d) T-RISs, $R = 150$ m.

Fig. 10. Overall connection probability vs. RIS size (number of elements on each RIS array is N_k, $\mu_r = 0.005/m^2$, and $\mu_o = 0.01/m^2$).

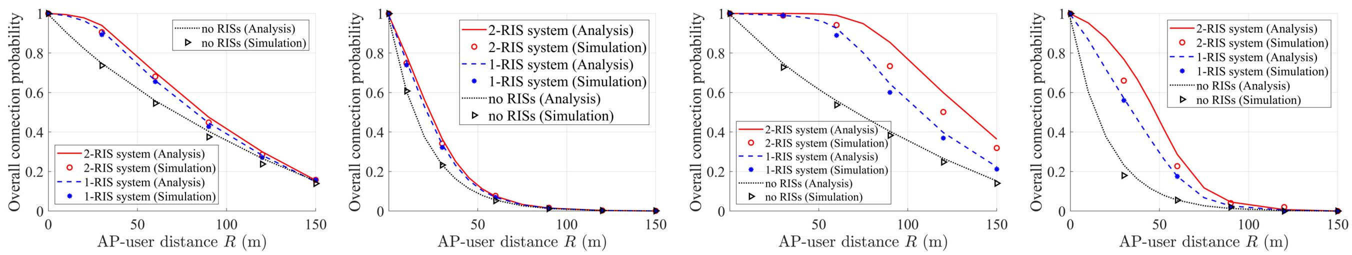

(a) R-RISs, $\mu_o = 0.01/m^2$. (b) R-RISs, $\mu_o = 0.05/m^2$. (c) T-RISs, $\mu_o = 0.01/m^2$. (d) T-RISs, $\mu_o = 0.05/m^2$.

Fig. 11. Overall connection probability vs. AP-user distance ($\mu_r = 0.005/m^2$, RIS array size $N_k = 64 \times 64$).

TABLE I
APPROXIMATED COVERAGE RATIO

	R-RISs $\mu_o = 0.01$	R-RISs $\mu_o = 0.05$	T-RISs $\mu_o = 0.01$	T-RISs $\mu_o = 0.05$
$\widehat{S}_0$	0.463	0.055	0.463	0.055
$\widehat{S}_1$	0.532	0.075	0.707	0.138
$\widehat{S}_2$	0.561	0.081	0.859	0.200

probability drops below 0.1, indicating that communication links can hardly be supported. In Fig. 11(b) and Fig. 11(d) which represent the higher obstacle density, the cut-off distance without RISs is approximately 48 m. This distance extends to about 53 m with R-RISs and nearly 70 m with T-RISs when single-RIS systems are used. When two-RIS systems are used, the cut-off distance extends to about 55 m with R-RISs and nearly 80 m with T-RISs. Thus, T-RISs demonstrate much better performance in extending communication distance.

(3) Enhancement in coverage ratio using RISs: As given by (19), the connection probability can be used to calculate the coverage ratio over a given area. Here, we use data points from Fig. 11 to evaluate the approximated coverage ratio according to (20). We focus on cases where $\mu_r = 0.005/m^2$, μ_o is chosen as $0.01/m^2$ or $0.05/m^2$, the RIS array size is 64×64, and the maximum distance R_{max} between the AP and the user is 120 m. In Table I, $\widehat{S}_m$ denotes the approximated coverage ratio where the system can support RIS links with at most m RISs and $m = 0$ indicates that no RISs are deployed. To approximate coverage ratio in a region with $R_{max} = 120$ m, five data points are chosen corresponding to AP-user distances of 0.01 m, 30 m, 60 m, 90 m, and 120 m. According to Table I, the coverage ratio increases by at least 14% in all the four cases when single-RIS links are used, and by at least 20% when both single-RIS and two-RIS links are used, which demonstrates the effectiveness of reducing uncovered regions through deployment of RISs. When T-RISs are used, the improvement is even more significant. For both obstacle densities, the coverage ratio improves by at least 50% when T-RISs are used. When two-RIS links with T-RISs are supported, the improvement is 86% with $\mu_o = 0.01/m^2$ and 264% with $\mu_o = 0.05/m^2$. This highlights the effectiveness of both T-RISs and two-RIS links in reaching NLOS regions, especially with a denser obstacle distribution.

D. Discussion

The main conclusions of this section, which again are based on assumptions of Poisson-distributed RISs and obstacles, Nakagami fading, and the sectored antenna model, are that 2-RIS links are valuable for longer-distance communications and that T-RISs significantly outperform R-RISs of the same size across all scenarios. However, system designers must take into account other factors when choosing what type of RIS to use and whether to support multi-RIS links. These other factors, which are difficult to quantify but are nonetheless important considerations, include added overhead for routing and beam alignment when using multi-RIS links and higher cost for manufacturing T-RISs compared to R-RISs. The relative connection probabilities across these different comparison points, which can be evaluated from our derived expressions, can help system designers decide whether the added cost/complexity are worth incurring for their particular environment.

VIII. CONCLUSION

In this paper, the connection probability of RIS-assisted communication was analyzed theoretically when R-RISs or T-RISs are used. The single-RIS link connection probability and an upper bound on multi-RIS link connection probability were derived in sparse obstacle scenarios to allow investigation

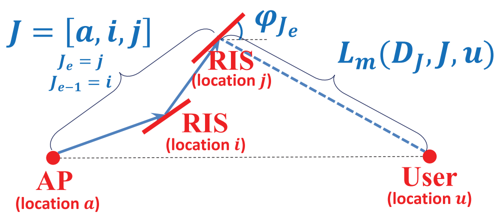

Fig. 12. Illustration of event $L_m(D_J, J, j)$ for proof of Lemma 4.

of the relationships among coverage performance, and RIS and obstacle distributions. Monte Carlo simulations validated the theoretical analysis for single-RIS and two-RIS links and allowed us to compare their relative benefits. We found that two-RIS links can improve coverage significantly for long-distance communication when medium to large sized RISs are deployed. However, for short-distance communication, the results show that single-RIS links are highly efficient and two-RIS links provide very little additional benefit. The results also demonstrated the power of T-RISs as compared to R-RISs. Generally, 1-RIS systems with T-RISs performed as well or better than 2-RIS systems with R-RISs. Alternatively, T-RISs can achieve the same connection probability as R-RISs with smaller array size and/or lower density.

Appendix A
Proof of Lemma 4

Let $d_{i,j}$ denote the distance between locations i and j, $g_{i,j}$ denote the small-scale channel gain on a link between locations i and j, and u and a denote the locations of the user and the AP, respectively. Let φ_j denote the orientation of RIS at location j. Additionally, let $J = [J_1, J_2, \ldots, J_{e-1}, J_e]$ be a vector representing the sequential locations of nodes (RISs, the user, or the AP) in a path starting from location J_1 and ending at location J_e, where J_{e-1} and J_e represent the last two node locations in J. An example of J is illustrated in Fig. 12, where $J = [a, i, j]$ represents a signal propagation path where the signal is transmitted from the AP to RIS at location i, and further propagates to RIS at location j.

In order to interpret $A_M(D_M, r_i, \theta_i|d_{a,u})$, three events are defined as follows:

1) Event R_i: there is an RIS located at location i, and the probability of its occurrence is $\mu_r \Delta h$ where $\Delta h \to 0$.
2) Event $L_{los}(i,j)$: there is a LOS link between location i and j, and the probability of its occurrence is $P_{los}(d_{i,j})$ according to (11).
3) Event $L_m(D_J, J, j)$: At least one m-RIS link exists between location J_e and j as illustrated in Fig. 12, and this m-RIS link should satisfy two conditions: a) $\frac{\prod_{i=1}^{m} G_s(\theta_i^r) G_s(\theta_i^t) \prod_{i=1}^{m+1} g_i}{\prod_{i=1}^{m+1} d_i^2} \geq D_J$ according to (17) where g_i and d_i are the small-scale channel gain and the distance of the ith path segment in the m-RIS link, respectively, and b) if an RIS is positioned at location J_e, it must have a proper orientation φ_{J_e} to receive signals from the device at location J_{e-1} and then transmit signals to the m-RIS link.

For ease of notation, let $c_J = L_{los}(J_e, J_{e-1}) \cap R_{J_e}$ and $b_J^m = L_m(D_J, J, u)$ where $D_J = D_M \prod_{i=1}^{|J|-1} d_{J_i,J_{i+1}}^2 / \prod_{i=1}^{|J|-1} g_{J_i,J_{i+1}}$. Then we have

$$P\Big(\overline{A_M(D_M, r_i, \theta_i|d_{a,u})}\Big) = \mathbb{E}_{g_{a,i}}\Big(P\big(\overline{c_{[a,i]} \cap b_{[a,i]}^{M-1}}|g_{a,i}\big)\Big). \tag{42}$$

For ease of notation for the following derivation, let $g_{\mathbf{Q}}^i$ denote all the small-scale channel gains $g_{i,j}$ such that $j \in \mathbf{Q}$. Since events $c_{[a,i]}$ and $b_{[a,i]}^{M-1}$ are independent due to independence assumption of LOS statuses and small-scale channel gains on different links, we have

$$\begin{aligned}
&P\Big(\bigcap_{i\in\mathbf{Q}} \overline{A_M(D_M, r_i, \theta_i|d_{a,u})}\Big)\\
&= \mathbb{E}_{g_{\mathbf{Q}}^a}\Big(P\big(\bigcap_{i\in\mathbf{Q}} \overline{A_M(D_M, r_i, \theta_i|d_{a,u})}|g_{\mathbf{Q}}^a\big)\Big)\\
&= \mathbb{E}_{g_{\mathbf{Q}}^a}\Big(P\big(\bigcap_{i\in\mathbf{Q}} \overline{c_{[a,i]}}|g_{\mathbf{Q}}^a\big)\\
&\quad + \sum_{j\in\mathbf{Q}} P\big(\bigcap_{\substack{i\in\mathbf{Q},\\ i\neq j}} \overline{c_{[a,i]}} \bigcap_{n\in\{j\}} c_{[a,n]} \cap \overline{b_{[a,n]}^{M-1}}|g_{\mathbf{Q}}^a\big)\\
&\quad + \sum_{\substack{j,k\in\mathbf{Q},\\ j\neq k}} P\big(\bigcap_{\substack{i\in\mathbf{Q},\\ i\neq j,k}} \overline{c_{[a,i]}} \bigcap_{n\in\{j,k\}} c_{[a,n]} \cap \overline{b_{[a,n]}^{M-1}}|g_{\mathbf{Q}}^a\big) + \cdots\\
&\quad + P\big(\bigcap_{n\in\mathbf{Q}} c_{[a,n]} \cap \overline{b_{[a,n]}^{M-1}}|g_{\mathbf{Q}}^a\big)\Big)\\
&= \mathbb{E}_{g_{\mathbf{Q}}^a}\Big(\prod_{i\in\mathbf{Q}} P\big(\overline{c_{[a,i]}}|g_{\mathbf{Q}}^a\big)\\
&\quad + \sum_{j\in\mathbf{Q}} \prod_{\substack{i\in\mathbf{Q},\\ i\neq j}} P\big(\overline{c_{[a,i]}}|g_{\mathbf{Q}}^a\big) \prod_{n\in\{j\}} P\big(c_{[a,n]}|g_{\mathbf{Q}}^a\big) P\big(\overline{b_{[a,n]}^{M-1}}|g_{\mathbf{Q}}^a\big)\\
&\quad + \sum_{\substack{j,k\in\mathbf{Q},\\ j\neq k}} \prod_{\substack{i\in\mathbf{Q},\\ i\neq j,k}} P\big(\overline{c_{[a,i]}}|g_{\mathbf{Q}}^a\big) \prod_{n\in\{j,k\}} P\big(c_{[a,n]}|g_{\mathbf{Q}}^a\big)\\
&\quad \times P\big(\bigcap_{n\in\{j,k\}} \overline{b_{[a,n]}^{M-1}}|g_{\mathbf{Q}}^a\big) + \cdots\\
&\quad + \prod_{n\in\mathbf{Q}} P\big(c_{[a,n]}|g_{\mathbf{Q}}^a\big) P\big(\bigcap_{n\in\mathbf{Q}} \overline{b_{[a,n]}^{M-1}}|g_{\mathbf{Q}}^a\big)\Big).
\end{aligned} \tag{43}$$

Similarly, $\prod_{i\in\mathbf{Q}} P\big(\overline{A_M(D_M, r_i, \theta_i|d_{a,u})}\big)$ shares the expression of (43), substituting the term $P\big(\bigcap_n \overline{b_{[a,n]}^{M-1}}|g_{\mathbf{Q}}^a\big)$ with $\prod_n P\big(\overline{b_{[a,n]}^{M-1}}|g_{\mathbf{Q}}^a\big)$. Therefore, we can show $P\big(\bigcap_J \overline{b_J^{M-1}}\big) > \prod_J P\big(\overline{b_J^{M-1}}\big)$ in order to show $P\big(\bigcap_{i\in\mathbf{Q}} \overline{A_M(D_M, r_i, \theta_i|d_{a,u})}\big) > \prod_{i\in\mathbf{Q}} P\big(\overline{A_M(D_M, r_i, \theta_i|d_{a,u})}\big)$ where $M \geq 2$, which will be demonstrated in the following.

Define $\mathbf{S} = \{(r,\theta)|r > 0, \theta \in [0, 2\pi)\}$ as the set of all possible RIS locations. Let $\mathbf{S}(\varphi_{J_e}, J) \subseteq \mathbf{S}$ denote the set of potential RIS locations, such that signals transmitted from location J_{e-1} can be received by RIS at J_e and then relayed to those potential RIS locations, assuming no signal blockage and that the orientation of the RIS at J_e is φ_{J_e}. Therefore, according to the law of total probability, $P(b_J^m)$ can be given by

$$P(b_J^m) = \mathbb{E}_{\varphi_{J_e}, g_{\mathbf{S}(\varphi_{J_e}, J)}^{J_e}}\Big($$

$$P\Big(\bigcap_{j\in\mathbf{S}(\varphi_{J_e},J)}\overline{c_{[J,j]}\cap b^{m-1}_{[J,j]}}\Big|\varphi_{J_e},g^{J_e}_{\mathbf{S}(\varphi_{J_e},J)})\Big). \tag{44}$$

For ease of notation, let $\varphi^1 = \{\varphi_{J_e}\}_{J\in\cup_i\mathbf{J}_i}$ and $\mathbf{g}^1 = \{g^{J_e}_{\mathbf{S}(\varphi_{J_e},J)}\}_{J\in\cup_i\mathbf{J}_i}$. Then we have

$$\begin{aligned}&P\Big(\bigcap_{\mathbf{J}\in\cup_i\mathbf{J}_i}\overline{b^m_J}\Big)\\&=\mathbb{E}_{\varphi^1,\mathbf{g}^1}\Big(\\&P\Big(\bigcap_{\mathbf{J}\in\cup_i\mathbf{J}_i}\bigcap_{\substack{j\in\\ \mathbf{S}(\varphi_{J_e},J)}}\overline{c_{[J,j]}}\cup(c_{[J,j]}\cap\overline{b^{m-1}_{[J,j]}})\Big|\boldsymbol{\varphi}^1,\mathbf{g}^1)\Big).\end{aligned} \tag{45}$$

With notation $\varphi^2 = \{\varphi_{J_e}\}_{J\in\mathbf{J}_i}$ and $\mathbf{g}^2 = \{g^{J_e}_{\mathbf{S}(\varphi_{J_e},J)}\}_{J\in\mathbf{J}_i}$, we have

$$\begin{aligned}&\prod_i P\Big(\bigcap_{J\in\mathbf{J}_i}\overline{b^m_J}\Big)\\&=\prod_i\mathbb{E}_{\varphi^2,\mathbf{g}^2}\Big(\\&P\Big(\bigcap_{J\in\mathbf{J}_i}\bigcap_{\substack{j\in\\ \mathbf{S}(\varphi_{J_e},J)}}\overline{c_{[J,j]}}\cup(c_{[J,j]}\cap\overline{b^{m-1}_{[J,j]}})\Big|\varphi^2,\mathbf{g}^2)\Big).\end{aligned} \tag{46}$$

Similar as the calculation in (43), we can show $P(\bigcap_{\mathbf{J}\in\cup_i\mathbf{J}'_i}\overline{b^{m-1}_J}) \geq \prod_i P(\bigcap_{J\in\mathbf{J}'_i}\overline{b^{m-1}_J})$ in order to show $P(\bigcap_{\mathbf{J}\in\cup_i\mathbf{J}_i}\overline{b^m_J}) > \prod_i P(\bigcap_{J\in\mathbf{J}_i}\overline{b^m_J})$. In other words, we only need to show $P(\bigcap_{\mathbf{J}\in\cup_i\mathbf{J}_i}\overline{b^0_J}) \geq \prod_i P(\bigcap_{J\in\mathbf{J}_i}\overline{b^0_J})$ in order to show $P\Big(\bigcap_{i\in\mathbf{Q}}\overline{A_M(D_M,r_i,\theta_i|d_{a,u})}\Big) > \prod_{i\in\mathbf{Q}}P\Big(\overline{A_M(D_M,r_i,\theta_i|d_{a,u})}\Big)$.

Let $S(D_J,J_e,j)$ represent the event that the $\frac{g_{J_e,j}}{d^2_{J_e,j}} \geq D_J$. Therefore, the expression of $P\big(\overline{b^0_J}\big)$ can be formulated similarly to that in (44) as follows

$$\begin{aligned}&P\big(\overline{b^0_J}\big)\\&=\mathbb{E}_{\varphi_{J_e}}\Big(P\Big(\bigcap_{\substack{j\in\{u\}\cap\\ \mathbf{S}(\varphi_{J_e},J)}}\overline{L_{los}(J_e,j)\cap S(D_J,J_e,j)}\Big|\varphi_{J_e})\Big).\end{aligned} \tag{47}$$

Similar as the processing in (45) and (46), we have $P(\bigcap_{\mathbf{J}\in\cup_i\mathbf{J}_i}\overline{b^0_J}) \geq \prod_i P(\bigcap_{J\in\mathbf{J}_i}\overline{b^0_J})$ since $P(\bigcap_{\mathbf{J}\in\cup_i\mathbf{J}_i}\overline{L_{los}(J_e,j)}) \geq \prod_i P(\bigcap_{J\in\mathbf{J}_i}\overline{L_{los}(J_e,j)})$ according to (11). In other words, $P\Big(\bigcap_{i\in\mathbf{Q}}\overline{A_M(D_M,r_i,\theta_i|d_{a,u})}\Big) > \prod_{i\in\mathbf{Q}}P\Big(\overline{A_M(D_M,r_i,\theta_i|d_{a,u})}\Big)$ can be proved.

Appendix B
Proof of Lemma 5

To interpret $A_M(D_M,r,\theta|R)$, let $I_{M-m}(D,\alpha_m,R)$ denote the event that there is at least one $(M-m)$-RIS link between the user and a given location for RIS m. This link must satisfy the condition of $\frac{\prod_{i=m}^M G_s(\theta_i^r)G_s(\theta_i^t)\prod_{i=m+1}^{M+1}g_i}{\prod_{i=m+1}^{M+1}d_i^2} \geq D$ according to (17). Herein, R is the distance between the user and this location for RIS m, and $\alpha_m \in [0,\pi]$ is the angle between the link from RIS m to the user and the link from RIS m to the previous device (RIS $(m-1)$ or the AP) as illustrated in Fig. 13.

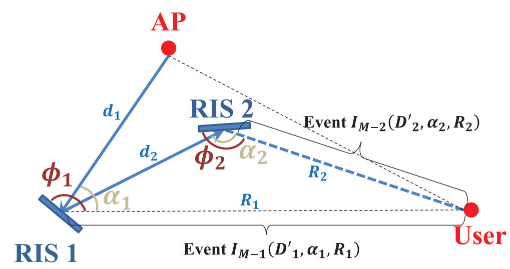

Fig. 13. Illustration of an RIS-assisted link for proof of Lemma 5.

Let ϕ_m denote the angle between the orientation of RIS m and the link from RIS m to the user as illustrated in Fig. 13. Then, the probability of event $A_M(D_M,r,\theta|R)$ occurring is given by

$$\begin{aligned}&P(A_M(D_M,r,\theta|R))\\&=\mu_r\Delta hP_{los}(r)\int_0^\infty f_g(x)\\&\quad\times P\Big(I_{M-1}(\frac{D_M}{x}r^2,\alpha_a(r,\theta,R),d(r,\theta,R))\Big)\mathrm{d}x\\&\overset{(a)}{=}\mu_r\Delta hP_{los}(r)\int_0^\infty f_g(x)\\&\quad\times\mathbb{E}_{\phi_1}\Big(P\big(I_{M-1}(\frac{D_M}{x}r^2,\alpha_a(r,\theta,R),d(r,\theta,R))|\phi_1\big)\Big)\mathrm{d}x,\end{aligned} \tag{48}$$

where $f_g(x)$ is given in (2), and (a) comes from the law of total probability. Let $W_{M-m}(D,\alpha,R) = \mathbb{E}_{\phi_m}\Big(P(I_{M-m}(D,\alpha,R)|\phi_m)\Big)$. Then $W_{M-m}(D,\alpha,R)$ depends on the type of utilized RISs, which is given as follows.

(1) R-RISs: Let $\eta^{\alpha_m}_{\phi_m}$ denote if RIS m has a proper orientation ϕ_m to face towards the previous device (RIS $(m-1)$ or the AP) given α_m, such that

$$\eta^{\alpha_m}_{\phi_m} = \begin{cases}1, & \text{if } \phi_m\in(\frac{\pi-\alpha_r}{2}+\alpha_m,\frac{\pi+\alpha_r}{2}+\alpha_m),\\0, & \text{otherwise.}\end{cases} \tag{49}$$

Then we have

$$\begin{aligned}&P(I_{M-m}(D,\alpha,R)|\phi_m)\\&=\eta^{\alpha}_{\phi_m}\Big(1-P\Big(\bigcap_{\substack{r\in(0,\infty),\\ \theta\in(\phi_m-\frac{\pi+\alpha_r}{2},\phi_m-\frac{\pi-\alpha_r}{2})}}\overline{A_{M-m}(D,r,\theta|R)}\Big)\Big)\\&\overset{(a)}{\leq}\eta^{\alpha}_{\phi_m}\Big(1-\prod_{\substack{r\in(0,\infty),\\ \theta\in(\phi_m-\frac{\pi+\alpha_r}{2},\phi_m-\frac{\pi-\alpha_r}{2})}}P\big(\overline{A_{M-m}(D,r,\theta|R)}\big)\Big)\\&=\eta^{\alpha}_{\phi_m}\Big(1-\prod_{\substack{r\in(0,\infty),\\ \theta\in(\phi_m-\frac{\pi+\alpha_r}{2},\phi_m-\frac{\pi-\alpha_r}{2})}}\exp\big(-\mu_r\Delta hP_{los}(r)\\&\quad\times\int_0^\infty f_g(x)W_{M-m-1}(\frac{Dr^2}{x},\alpha_a(r,\theta,R),d(r,\theta,R))\mathrm{d}x\big)\Big)\end{aligned}$$

$$= \eta_{\phi_m}^{\alpha}\Big(1 - \exp\big(-\int_{\phi_m - \frac{\pi+\alpha_r}{2}}^{\phi_m - \frac{\pi-\alpha_r}{2}} \int_0^{\infty} \mu_r P_{los}(r) \times \int_0^{\infty} f_g(x) W_{M-m-1}(\frac{Dr^2}{x}, \alpha_a(r,\theta,R), d(r,\theta,R)) \times r\,\mathrm{d}x\,\mathrm{d}r\,\mathrm{d}\theta\big)\Big), \tag{50}$$

where (a) comes from Lemma 4. Furthermore, $W_{M-m}(D,\alpha,R)$ can be calculated as follows

$$\begin{aligned} &W_{M-m}(D,\alpha,R) \\ &= \mathbb{E}_{\phi_m}\Big(P\big(I_{M-m}(D,\alpha,R)|\phi_m\big)\Big) \\ &= \frac{1}{2\pi}\int_{\alpha+\frac{\pi-\alpha_r}{2}}^{\alpha+\frac{\pi+\alpha_r}{2}} \Big(1 - \exp\big(-\int_{\phi_m - \frac{\pi+\alpha_r}{2}}^{\phi_m - \frac{\pi-\alpha_r}{2}} \\ &\quad \int_0^{\infty} \mu_r P_{los}(r) \int_0^{\infty} \\ &\quad f_g(x) W_{M-m-1}(\frac{Dr^2}{x}, \alpha_a(r,\theta,R), d(r,\theta,R)) \\ &\quad \times r\,\mathrm{d}x\,\mathrm{d}r\,\mathrm{d}\theta\big)\Big)\mathrm{d}\phi_m \\ &\overset{(a)}{<} \frac{\alpha_r}{2\pi} - \frac{\alpha_r}{2\pi}\exp\Big(-\frac{1}{\alpha_r}\int_{\alpha+\frac{\pi-\alpha_r}{2}}^{\alpha+\frac{\pi+\alpha_r}{2}} \\ &\quad \big(\int_{\phi_m - \frac{\pi+\alpha_r}{2}}^{\phi_m - \frac{\pi-\alpha_r}{2}} \int_0^{\infty} \mu_r P_{los}(r) \int_0^{\infty} f_g(x) \\ &\quad \times W_{M-m-1}(\frac{Dr^2}{x}, \alpha_a(r,\theta,R), d(r,\theta,R)) \\ &\quad \times r\,\mathrm{d}x\,\mathrm{d}r\,\mathrm{d}\theta\big)\mathrm{d}\phi_m\Big), \end{aligned} \tag{51}$$

where (a) comes from Jensen's inequality. Then the result in (35) can be acquired.

(2) T-RISs: Since T-RISs can redirect signals to both sides, then $\eta_{\phi_m}^{\alpha_m}$ is given by

$$\eta_{\phi_m}^{\alpha_m} = \begin{cases} 1, & \text{if } \phi_m \in (\frac{\pi-\alpha_r}{2}+\alpha_m, \frac{\pi+\alpha_r}{2}+\alpha_m) \cup \\ & \quad (\frac{3\pi-\alpha_r}{2}+\alpha_m, \frac{3\pi+\alpha_r}{2}+\alpha_m), \\ 0, & \text{otherwise.} \end{cases} \tag{52}$$

Then $W_{M-m}(D,\alpha,R)$ can be calculated as follows

$$\begin{aligned} &W_{M-m}(D,\alpha,R) \\ &= \frac{1}{\pi}\int_{\alpha+\frac{\pi-\alpha_r}{2}}^{\alpha+\frac{\pi+\alpha_r}{2}} \Big(1 - \exp\big(\\ &\quad -\int_{\phi_m - \frac{\pi+\alpha_r}{2}}^{\phi_m - \frac{\pi-\alpha_r}{2}} \int_0^{\infty} \mu_r P_{los}(r) \int_0^{\infty} f_g(x) \\ &\quad \times W_{M-m-1}(\frac{Dr^2}{x}, \alpha_a(r,\theta,R), d(r,\theta,R)) r\,\mathrm{d}x\,\mathrm{d}r\,\mathrm{d}\theta \\ &\quad -\int_{\phi_m - \frac{\pi+\alpha_r}{2}+\pi}^{\phi_m - \frac{\pi-\alpha_r}{2}+\pi} \int_0^{\infty} \mu_r P_{los}(r) \int_0^{\infty} f_g(x) \\ &\quad \times W_{M-m-1}(\frac{Dr^2}{x}, \alpha_a(r,\theta,R), d(r,\theta,R)) \\ &\quad \times r\,\mathrm{d}x\,\mathrm{d}r\,\mathrm{d}\theta\big)\Big)\mathrm{d}\phi_m \\ &\overset{(a)}{<} \frac{\alpha_r}{\pi} - \frac{\alpha_r}{\pi}\exp\Big(\\ &\quad -\frac{1}{\alpha_r}\int_{\alpha+\frac{\pi-\alpha_r}{2}}^{\alpha+\frac{\pi+\alpha_r}{2}} \big(\int_{\phi_m - \frac{\pi+\alpha_r}{2}}^{\phi_m - \frac{\pi-\alpha_r}{2}} \int_0^{\infty} \mu_r P_{los}(r) \\ &\quad \times \int_0^{\infty} f_g(x) W_{M-m-1}(\frac{Dr^2}{x}, \alpha_a(r,\theta,R), d(r,\theta,R)) \\ &\quad \times r\,\mathrm{d}x\,\mathrm{d}r\,\mathrm{d}\theta \\ &\quad -\int_{\phi_m - \frac{\pi+\alpha_r}{2}+\pi}^{\phi_m - \frac{\pi-\alpha_r}{2}+\pi} \int_0^{\infty} \mu_r P_{los}(r) \int_0^{\infty} f_g(x) \\ &\quad \times W_{M-m-1}(\frac{Dr^2}{x}, \alpha_a(r,\theta,R), d(r,\theta,R)) \\ &\quad \times r\,\mathrm{d}x\,\mathrm{d}r\,\mathrm{d}\theta\big)\mathrm{d}\phi_m\Big), \end{aligned} \tag{53}$$

where (a) comes from Jensen's inequality. Then the result in (37) can be acquired.

REFERENCES

[1] T. S. Rappaport, J. N. Murdock, and F. Gutierrez, "State of the art in 60-GHz integrated circuits and systems for wireless communications," *Proc. IEEE*, vol. 99, no. 8, pp. 1390–1436, Aug. 2011.

[2] T. Bai and R. W. Heath, "Coverage and rate analysis for millimeter-wave cellular networks," *IEEE Trans. Wireless Commun.*, vol. 14, no. 2, pp. 1100–1114, Feb. 2015.

[3] A. V. Alejos, M. G. Sanchez, and I. Cuinas, "Measurement and analysis of propagation mechanisms at 40 GHz: Viability of site shielding forced by obstacles," *IEEE Trans. Veh. Technol.*, vol. 57, no. 6, pp. 3369–3380, Nov. 2008.

[4] E. Basar, I. Yildirim, and F. Kilinc, "Indoor and outdoor physical channel modeling and efficient positioning for reconfigurable intelligent surfaces in mmWave bands," *IEEE Trans. Commun.*, vol. 69, no. 12, pp. 8600–8611, Dec. 2021.

[5] N. S. Perovic, M. D. Renzo, and M. F. Flanagan, "Channel capacity optimization using reconfigurable intelligent surfaces in indoor mmWave environments," in *Proc. IEEE Int. Conf. Commun. (ICC)*, Jun. 2020, pp. 1–7.

[6] A. M. Elbir, A. Papazafeiropoulos, P. Kourtessis, and S. Chatzinotas, "Deep channel learning for large intelligent surfaces aided mm-Wave massive MIMO systems," *IEEE Wireless Commun. Lett.*, vol. 9, no. 9, pp. 1447–1451, Sep. 2020.

[7] D. Kudathanthirige, D. Gunasinghe, and G. Amarasuriya, "Performance analysis of intelligent reflective surfaces for wireless communication," in *Proc. IEEE Int. Conf. Commun. (ICC)*, Aug. 2020, pp. 1–6.

[8] H. Du, J. Zhang, J. Cheng, and B. Ai, "Millimeter wave communications with reconfigurable intelligent surfaces: Performance analysis and optimization," *IEEE Trans. Commun.*, vol. 69, no. 4, pp. 2752–2768, Apr. 2021.

[9] Y. Liu et al., "STAR: Simultaneous transmission and reflection for 360° coverage by intelligent surfaces," *IEEE Wireless Commun.*, vol. 28, no. 6, pp. 102–109, Dec. 2021.

[10] S. Zhang et al., "Intelligent omni-surfaces: Ubiquitous wireless transmission by reflective-refractive metasurfaces," *IEEE Trans. Wireless Commun.*, vol. 21, no. 1, pp. 219–233, Jan. 2022.

[11] E. Basar and H. V. Poor, "Present and future of reconfigurable intelligent surface-empowered communications [perspectives]," *IEEE Signal Process. Mag.*, vol. 38, no. 6, pp. 146–152, Nov. 2021.

[12] Z. Li, H. Hu, J. Zhang, and J. Zhang, "Coverage analysis of multiple transmissive RIS-aided outdoor-to-indoor mmWave networks," *IEEE Trans. Broadcast.*, vol. 68, no. 4, pp. 935–942, Dec. 2022.

[13] Y. Cao, T. Lv, and W. Ni, "Intelligent reflecting surface aided multi-user mmWave communications for coverage enhancement," in *Proc. IEEE 31st Annu. Int. Symp. Pers., Indoor Mobile Radio Commun.*, Aug. 2020, pp. 1–6.

[14] G. Lee, M. Jung, A. T. Z. Kasgari, W. Saad, and M. Bennis, "Deep reinforcement learning for energy-efficient networking with reconfigurable intelligent surfaces," in *Proc. IEEE Int. Conf. Commun. (ICC)*, Jun. 2020, pp. 1–6.

[15] W. Mei and R. Zhang, “Multi-beam multi-hop routing for intelligent reflecting surfaces aided massive MIMO,” *IEEE Trans. Wireless Commun.*, vol. 21, no. 3, pp. 1897–1912, Mar. 2022.
[16] C. Huang et al., “Multi-hop RIS-empowered terahertz communications: A DRL-based hybrid beamforming design,” *IEEE J. Sel. Areas Commun.*, vol. 39, no. 6, pp. 1663–1677, Jun. 2021.
[17] Y. Liu, Y. Jian, R. Sivakumar, and D. M. Blough, “Optimal access point placement for multi-AP mmWave WLANs,” in *Proc. 22nd Int. ACM Conf. Model., Anal. Simul. Wireless Mobile Syst.*, Nov. 2019, pp. 35–44.
[18] D. Kumar, J. Kaleva, and A. Tölli, “Blockage-aware reliable mmWave access via coordinated multi-point connectivity,” *IEEE Trans. Wireless Commun.*, vol. 20, no. 7, pp. 4238–4252, Jul. 2021.
[19] S. Biswas, S. Vuppala, J. Xue, and T. Ratnarajah, “On the performance of relay aided millimeter wave networks,” *IEEE J. Sel. Topics Signal Process.*, vol. 10, no. 3, pp. 576–588, Apr. 2016.
[20] Y. Yan, Q. Hu, and D. M. Blough, “Path selection with amplify and forward relays in mmWave backhaul networks,” in *Proc. IEEE 29th Annu. Int. Symp. Pers., Indoor Mobile Radio Commun. (PIMRC)*, vol. 7, Sep. 2018, pp. 1–6.
[21] S. Wu, R. Atat, N. Mastronarde, and L. Liu, “Improving the coverage and spectral efficiency of millimeter-wave cellular networks using device-to-device relays,” *IEEE Trans. Commun.*, vol. 66, no. 5, pp. 2251–2265, May 2018.
[22] W. Khawaja, O. Ozdemir, Y. Yapici, F. Erden, and I. Guvenc, “Coverage enhancement for NLOS mmWave links using passive reflectors,” *IEEE Open J. Commun. Soc.*, vol. 1, pp. 263–281, 2020.
[23] C. K. Anjinappa, F. Erden, and I. Güvenç, “Base station and passive reflectors placement for urban mmWave networks,” *IEEE Trans. Veh. Technol.*, vol. 70, no. 4, pp. 3525–3539, Apr. 2021.
[24] Z. Peng et al., “An effective coverage scheme with passive-reflectors for urban millimeter-wave communication,” *IEEE Antennas Wireless Propag. Lett.*, vol. 15, pp. 398–401, 2016.
[25] A. Deng, Y. Liu, and D. M. Blough, “Maximizing coverage for mmWave WLANs with dedicated reflectors,” in *Proc. IEEE Int. Conf. Commun. (ICC)*, Jun. 2021, pp. 1–6.
[26] J. Zhang and D. M. Blough, “Optimizing coverage with intelligent surfaces for indoor mmWave networks,” in *Proc. IEEE Conf. Comput. Commun. (IEEE INFOCOM)*, May 2022, pp. 830–839.
[27] H. Qin, Z. Liu, and C. Yang, “Indoor mm-wave coverage enhancement: Reconfigurable intelligent surface deployment strategy based on human mobility model,” *IEEE Commun. Lett.*, vol. 26, no. 10, pp. 2475–2479, Oct. 2022.
[28] M. He, W. Xu, and C. Zhao, “RIS-assisted broad coverage for mmWave massive MIMO system,” in *Proc. IEEE Int. Conf. Commun. Workshops (ICC Workshops)*, Jun. 2021, pp. 1–6.
[29] W. Qingqing and Z. Rui, “Towards smart and reconfigurable environment: Intelligent reflecting surface aided wireless network,” *IEEE Commun. Mag.*, vol. 58, no. 1, pp. 106–112, Jan. 2019.
[30] S. Zeng et al., “Reconfigurable intelligent surfaces in 6G: Reflective, transmissive, or both?” *IEEE Commun. Lett.*, vol. 25, no. 6, pp. 2063–2067, Jun. 2021.
[31] V. K. Chapala and S. M. Zafaruddin, “Reconfigurable intelligent surface empowered multi-hop transmission over generalized fading,” in *Proc. IEEE 95th Veh. Technol. Conf. (VTC-Spring)*, Jun. 2022, pp. 1–5.
[32] M. D. Renzo and J. Song, “Reflection probability in wireless networks with metasurface-coated environmental objects: An approach based on random spatial processes,” *EURASIP J. Wireless Commun. Netw.*, vol. 2019, p. 99, Apr. 2019, doi: 10.1186/S13638-019-1403-7.
[33] M. A. Kishk and M.-S. Alouini, “Exploiting randomly located blockages for large-scale deployment of intelligent surfaces,” *IEEE J. Sel. Areas Commun.*, vol. 39, no. 4, pp. 1043–1056, Apr. 2021.
[34] W. Tang et al., “Path loss modeling and measurements for reconfigurable intelligent surfaces in the millimeter-wave frequency band,” *IEEE Trans. Commun.*, vol. 70, no. 9, pp. 6259–6276, Sep. 2022.
[35] E. Björnson, Ö. T. Demir, and L. Sanguinetti, “A primer on near-field beamforming for arrays and reconfigurable intelligent surfaces,” in *Proc. 55th Asilomar Conf. Signals Syst. Comput.*, Nov. 2021, pp. 105–112.
[36] S. Hu, M. C. Ilter, and H. Wang, “Near-field beamforming for large intelligent surfaces,” in *Proc. IEEE 33rd Annu. Int. Symp. Pers., Indoor Mobile Radio Commun. (PIMRC)*, Sep. 2022, pp. 1367–1373.
[37] J. Zhang and D. M. Blough, “Coverage analysis for multi-hop communication in intelligent-surface-assisted mmWave WLANs,” in *Proc. IEEE 48th Conf. Local Comput. Netw. (LCN)*, Oct. 2023, pp. 1–9.
[38] T. Bai, R. Vaze, and R. W. Heath Jr., “Analysis of blockage effects on urban cellular networks,” *IEEE Trans. Wireless Commun.*, vol. 13, no. 9, pp. 5070–5083, Sep. 2014.
[39] T. Shafique, H. Tabassum, and E. Hossain, “Stochastic geometry analysis of IRS-assisted downlink cellular networks,” *IEEE Trans. Commun.*, vol. 70, no. 2, pp. 1442–1456, Feb. 2022.
[40] M. S. Zia, D. M. Blough, and M. A. Weitnauer, “Effects of SNR-dependent beam alignment errors on millimeter-wave cellular networks,” *IEEE Trans. Veh. Technol.*, vol. 71, no. 5, pp. 5216–5230, May 2022.
[41] P. S. Bithas, A. G. Kanatas, D. B. da Costa, P. K. Upadhyay, and U. S. Dias, “On the double-generalized gamma statistics and their application to the performance analysis of V2V communications,” *IEEE Trans. Commun.*, vol. 66, no. 1, pp. 448–460, Jan. 2018.
[42] H. Bateman and B. M. Project, *Higher Transcendental Functions*. New York, NY, USA: McGraw-Hill, 1953.
[43] J. An et al., “Stacked intelligent metasurfaces for multiuser beamforming in the wave domain,” in *Proc. IEEE Int. Conf. Commun. (ICC)*, Sep. 2023, pp. 2834–2839.
[44] D. Cruz-Uribe and C. J. Neugebauer, “Sharp error bounds for the trapezoidal rule and Simpson’s rule,” *J. Inequal. Pure Appl. Math.*, vol. 3, no. 4, pp. 1–22, 2002.
[45] P. A. W. Lewis and G. S. Shedler, “Simulation of nonhomogeneous Poisson processes by thinning,” *Nav. Res. Logistics Quart.*, vol. 26, no. 3, pp. 403–413, Sep. 1979.

Jingyuan Zhang (Graduate Student Member, IEEE) received the B.E. degree from Southeast University, China, in 2018, and the M.S. degree in electrical and computer engineering from Georgia Institute of Technology, Atlanta, GA, USA, in 2021, where she is currently pursuing the Ph.D. degree in electrical and computer engineering. Her current research interests include wireless communication and sensing assisted by intelligent surfaces.

Douglas M. Blough (Senior Member, IEEE) received the B.S. degree in electrical engineering and the M.S. and Ph.D. degrees in computer science from Johns Hopkins University, Baltimore, MD, USA, in 1984, 1986, and 1988, respectively. He is currently a Professor of electrical and computer engineering with Georgia Institute of Technology, Atlanta, GA, USA, where he also holds an adjunct position in computer science. His research interests include advanced wireless networks and dependability. He has been on the technical program committees of numerous conferences, including DSN, MobiHoc, MobiCom, MASS, Infocom, and ICDCS. He has held several editorial positions in the past and is currently on the editorial board of IEEE TRANSACTIONS ON WIRELESS COMMUNICATIONS.